BAR-ILAN UNIVERSITY

Giant Planar Hall Effect in Manganites

YOSI BASON

Submitted to the Senate of Bar-Ilan University,Ramat-Gan, Israel

Ramat-Gan, Israel February 2009

This work was carried out under the supervision of

Professor Lior Klein

Department of Physics

Bar-Ilan University

Acknowledgments

I would like to express my gratitude to my advisor, Prof. Lior Klein, whose expertise and patience added considerably to my graduate experience. I appreciate his vast knowledge and skill in many areas, and his assistance and support. I feel very fortunate that I was his student.

I also want to thank Nati Naftalis who cooperated with me during the last year on several projects, and contributed much to the work presented here.

I would like to acknowledge Prof. Charles Ahn and his students Jeng-Bang Yau, Xia Hong, and Jason Hoffman from the Applied Physics department at Yale who made the samples needed for my research, worked with me on several manuscripts, and also accompanied me during my visits there.

It has been a great pleasure to me to work with other members of my research group: Michael Feigenson, Moty Schultz, Isasechar Genish, Snir Seri, Nati Naftalis and Yishi Shperber.

I want to thank my family who helped me and supported me during my years of studies.

Finally, I want to thank my wife, Dorit, who was always there to listen to me talk about my experiments and research, and for her unabated support, diligence, and dedication to our family.

Contents

Abstract **i**

1 Scientific Background **1**
1.1 Magnetic Anisotropy . . . 1
1.1.1 Shape Anisotropy . . . 1
1.1.2 Magnetocrystalline Anisotropy . . . 2
1.1.3 Anisotropy Energy . . . 2
1.1.4 Magnetization Switching . . . 4
1.2 Anisotropic Magnetoresistance and Planar Hall Effect . . . 6
1.2.1 Physical Origin . . . 6
1.2.2 Mathematical Analysis . . . 8
1.2.3 Giant Planar Hall Effect . . . 9
1.2.4 Planar Hall effect switching . . . 12
1.2.5 Higher order Equations . . . 14
1.3 Spintronics . . . 18
1.3.1 Giant Magnetoresistance . . . 19
1.3.2 Tunneling Magnetoresistance . . . 19
1.3.3 Magnetic Random Access Memory . . . 20
1.3.4 GPHE based MRAM . . . 23

2 Materials **24**
2.1 Manganites . . . 24
2.1.1 Colossal Magnetoresistance . . . 24
2.1.2 Crystal Structure . . . 26
2.1.3 Phase Diagrams . . . 26
2.1.4 Electronic State and Double Exchange Model . . . 27
2.2 Magnetite . . . 30

3 Experimental details **32**
3.1 Film Fabrication . . . 32
3.1.1 Manganites . . . 32
3.1.2 Magnetite . . . 33

3.2 Sample Preparation 33
3.3 Equipment 35
3.4 Data Analysis 36

4 List of Publications **39**

5 Manuscripts **40**
5.1 Giant planar Hall effect in colossal magnetoresistive $La_{0.84}Sr_{0.16}MnO_3$ thin films 40
5.2 Characterization of the magnetic anisotropy in thin films of $La_{1-x}Sr_xMnO_3$ using the planar Hall effect 44
5.3 Planar Hall-effect magnetic random access memory 48
5.4 Planar Hall effect in epitaxial thin films of magnetite 52
5.5 The magnetoresistance tensor of $La_{0.8}Sr_{0.2}MnO_3$ 55

Bibliography **61**

Abstract

Although known for half a century, the planar Hall effect (PHE) is relatively less known than the ordinary and extraordinary Hall effects. The origin of the PHE is in the dependence of the resistivity on the orientation of the magnetic field and/or the internal magnetization. It appears in magnetic and non-magnetic metals and semiconductors. In magnetic conductors, the dominant effect leading to PHE is the dependence of the resistivity on the orientation of the internal magnetization relative to the current direction. This effect is known as spontaneous resistivity anisotropy or anisotropic magnetoresistance (AMR).

The AMR is a spin-orbit effect; however, the specific mechanism is system dependent. In itinerant ferromagnetic $3d$ alloys with exchange split bands the AMR is commonly interpreted in the framework of Mott's two current model: spin-up channel and spin-down channel. In these systems the AMR is attributed to the effect of the angle between the magnetic orientation and the current direction on the final state density available for the scattered charge carriers.

The AMR yields a transverse "Hall-like" field if $\mathbf{J}$ is neither parallel nor perpendicular to $\mathbf{M}$. Assuming $\mathbf{J} = \mathbf{J_x}\hat{\mathbf{x}}$ and $\mathbf{M}$ is in the $x-y$ plane with an angle φ relative to $\mathbf{J}$, the generated electric field has both longitudinal $E_x = \rho_\perp J_x + (\rho_\parallel - \rho_\perp) J_x \cos^2\varphi$, and transverse $E_y = (\rho_\parallel - \rho_\perp) J_x \sin\varphi \cos\varphi$ components, where E_y is the PHE field.

Although these simple equations are expected to hold only for amorphous materials, they have been used to describe the PHE and AMR even in epitaxial films, despite some discrepancies which were left unattended.

The PHE in magnetic materials has a small magnitude and therefore attracted little attention since its discovery. Recently, new interest in PHE emerged following study of magnetic semiconductor (Ga,Mn)As. The researchers found that PHE in (Ga,Mn)As is four orders of magnitude larger than what was previously observed and thus termed it the "Giant Planar Hall effect" (GPHE). They also pointed out the enormous application potential of this phenomenon, particulary in the fast developing field of spin-selective electronics known as 'spintronics', provided the obstacle of the relatively low Curie temperature $\sim$ 50K of (Ga,Mn)As is overcome.

This work started with our discovery of GPHE in manganite films. We found out that thin films of $La_{1-x}Sr_xMnO_3$ (LSMO) with a doping level of x=0.16 exhibit GPHE. The GPHE in manganite films is of comparable magnitude to that found in (Ga,Mn)As, and it is also observed in much higher temperatures of up to $\sim$ 140 K. This study was published in "Giant planar Hall effect in colossal magnetoresistive $La_{0.84}Sr_{0.16}MnO_3$ thin films", Y. bason, L. Klein, J.-B. Yau, X. Hong, and C. H. Ahn, Appl. Phys. Lett. **84**, 2593 (2004).

Since the PHE depends on the in-plane magnetization orientation, we used this effect to probe locally the in-plane magnetization orientation and in-plane magnetocrystalline anisotropy of manganite films. This study was published in "Characterization of the magnetic anisotropy in thin films of $La_{1-x}Sr_xMnO_3$ using the planar Hall effect", Y. Bason, L. Klein, J.-B. Yau, X. Hong, C. H. Ahn, Phys. Stat. Sol. (c)

1, No. 12, 3336-3338 (2004).

A more applicative use of the GPHE is magnetic random access memory (MRAM), which has attractive properties among various technologies considered for future memory applications, since in addition to being nonvolatile with high endurance, it can also be as fast as static random access memory and as dense as dynamic random access memory. Storing data in a typical MRAM device is accomplished by applying a magnetic field and causing a magnetic layer in the device to be magnetized in one of two possible states. Reading the data stored in a MRAM device requires reading the electrical resistance of the device, which depends on the magnetization orientation. Currently developed MRAM devices are based on magnetic tunnel junctions (MTJ). Current MTJ devices can achieve a $\sim$ 200% resistance difference between their two states; however, they are quite complicated to fabricate and in addition both magnetic states have the same sign of measured voltage. We suggested a different approach for storing and reading a magnetic bit using the GPHE, and demonstrated this idea with manganite films at temperatures above room temperature. This work was published in "Planar Hall-effect magnetic random access memory", Y. Bason, L. Klein, J.-B. Yau, X. Hong, J. Hoffman and C. H. Ahn, J. Appl. Phys. **99**, 08R701 (2006).

We also examined the use of another epitaxial film, Fe_3O_4 (magnetite), as the basis for a PHE-MRAM device. The magnetite films shows GPHE at temperatures even higher than the manganite with optimal doping of x=0.35 used before. Moreover, the PHE magnitude in magnetite is more stable at the room temperature range. We reported on GPHE in magnetite film and demonstrated one magnetic bit stability over time. This work was published in "Planar Hall effect in epitaxial thin films of

magnetite", Y. Bason, L. Klein, H. Q. Wang, J. Hoffman, X. Hong, V. E. Henrich, and C. H. Ahn, J. Appl. Phys. **101**, 9J507 (2007).

As noted before, the simple equations that describe the AMR and PHE are expected to hold only for amorphous films. Nevertheless, they have been used to describe AMR and PHE in films of manganites and other epitaxial materials while qualitative and quantitative deviations were occasionally attributed to extrinsic effects. In a previous work, "Giant planar Hall effect in colossal magnetoresistive $La_{0.84}Sr_{0.16}MnO_3$ thin films", it was noted that while we could use the simple equations to fit AMR and PHE data of manganite films, the term $(\rho_{\parallel} - \rho_{\perp})$ in the AMR equation differed from $(\rho_{\parallel} - \rho_{\perp})$ in the PHE equation, and we suggested that the source of the inconsistency might be crystalline contributions. The role of the crystal symmetry was the topic of our last publication in which we formulated new equations that describe the AMR and PHE in manganites by expanding the resistivity tensor to the 4th order and keeping terms consistent with crystal symmetry. These new equations address all the discrepancies previously reported for manganites and other epitaxial films. This work is entitled "The magnetoresistance tensor of $La_{0.8}Sr_{0.2}MnO_3$", Y. Bason, J. Hoffman, C. H. Ahn, and L. Klein and it submitted to PRB.

In summery, this thesis includes the discovery of the giant planar Hall effect in manganites, the use of the effect for magnetic characterization and for devices such as MRAM and finally the derivation of equations that provide a comprehensive description of the effect for any current direction.

Chapter 1

Scientific Background

1.1 Magnetic Anisotropy

The preference of the magnetization of a ferromagnetic sample to lie along a particular direction (or directions) is called magnetic anisotropy, and the preferred directions are called the easy axes of the magnetization. In the absence of an external magnetic field, the magnetization in a ferromagnetic material would be along one of the easy axes of the magnetization, and changing its direction by applying an external field would require overcoming the magnetic anisotropy. Magnetic anisotropy has two main sources: shape anisotropy and magnetocrystalline anisotropy.

1.1.1 Shape Anisotropy

The magneto-static energy of a non-spherical ferromagnetic sample depends on the magnetic direction. Therefore a non-spherical ferromagnetic is magnetically anisotropic with easy axis along its longer axis. When a magnetized sample has surfaces through which flux lines emerge with a normal component, "free poles" exist at the end surfaces. A magnetic field emanates from the north poles and terminates at the south poles. Depending on the shape and aspect ratio of the sample, the clos-

ing path of least energy for part of this dipole field is through the sample. When this field passes through the sample, it opposes the magnetization that set up the surface poles in the first place. This field is called the demagnetizing field. Its strength and direction generally vary with position inside samples but are often assumed to be constant. The demagnetizing field strength depends on the number of "free poles", therefore, it is stronger when the end surface of the sample is bigger, i.e., along the short axis of the sample.

1.1.2 Magnetocrystalline Anisotropy

Magnetocrystalline anisotropy (MCA) originates from the coupling of the spin part of the magnetic moment to the electronic orbital shape and orientation (spin-orbit coupling) as well as in the chemical bonding of the orbitals on a given atom with their local environment (crystalline electric field). If the local crystal field seen by an atom is of low symmetry and if the bonding electrons of that atom have an asymmetric charge distribution ($L_z \neq 0$), then the atomic orbitals interact anisotropically with the crystal field, meaning that certain orientations for the molecular orbitals or bonding electron charge distributions are energetically preferred.

1.1.3 Anisotropy Energy

The phenomenological description of the anisotropy depends on the symmetry of the anisotropy.

- **Uniaxial Anisotropy:** Uniaxial anisotropy corresponds to the situation where only one easy axis of magnetization exists. For sake of simplicity, we assume that the easy axis direction coincides with the cartesian z axis. The uniaxial

crystal anisotropy energy density is usually expressed as a power series of the form:

$$u_a = K_{u0} + K_{u1}\sin^2\alpha + K_{u2}\sin^4\alpha + \ldots \tag{1.1}$$

where $K_{u0}, K_{u1}, K_{u2}, \ldots$, are the anisotropy constants having the dimensions of energy per unit volume, and α is the angle between the magnetization and the z axis. The coefficient K_{u0} has no meaning for anisotropic properties because it is independent of the orientation of $\mathbf{M}$. For our purposes it is sufficient to truncate the expansion after the $\sin^2\alpha$ term. In this case the anisotropic behavior depends on the sign of the constant K_{u1}. When $K_{u1} > 0$, the anisotropy energy admits two minima at $\alpha = 0$ and $\alpha = \pi$, that is, when the magnetization lies along the positive or negative z axis. This case is referred to as easy axis anisotropy. Conversely, when $K_{u1} < 0$ the energy is minimized for $\alpha = \pi/2$, meaning that any direction in the $x - y$ plane corresponds to an easy direction. This case is often referred to as easy plane anisotropy.

- **Biaxial Anisotropy:** When the anisotropy energy density has cubic symmetry, a typical expansion of the anisotropy energy density is:

$$u_a^{cubic} = K_0 + K_1(\alpha_1^2\alpha_2^2 + \alpha_2^2\alpha_3^2 + \alpha_3^2\alpha_1^2) + K_2(\alpha_1^2\alpha_2^2\alpha_3^2) + \ldots, \tag{1.2}$$

where $K_0, K_1, K_2, \ldots$ are the anisotropy constants and α_1, α_2 and α_3 are cosines of the angles between the magnetization and the crystal axes. As before, we neglect terms of order greater than fourth (i.e., $K_2 = 0$, etc.). When $K_1 > 0$, there are six equivalent energy minima corresponding to the directions x, y, z, both positive and negative. Conversely, when $K_1 < 0$ there are eight equiva-

lent minima along directions pointing to the vertices of the cube, the $\langle 1,1,1\rangle$ directions, while the coordinate axes become hard axes.

Superposition of Uniaxial and Bi-Axial anisotropies

The anisotropy energy of a two dimensional sample with both uniaxial and bi-axial anisotropies is given by:

$$u = K_0 + K_{u1}\sin^2\alpha + K_1\cos^2 2\alpha \tag{1.3}$$

The first term is related to the uniaxial anisotropy, and minimizes along $\alpha = 0, \pi$, and the second term is related to the bi-axial anisotropy and minimizes along $\alpha = \pm\pi/4, \pm 3\pi/4$. The easy axes directions of the system are the directions of minimum energy and can be found by minimizing Eq. 1.3 with respect to α using the conditions $\partial u/\partial\alpha = 0$ and $\partial^2 u/\partial\alpha^2 > 0$. Due to the competition between the uniaxial and the bi-axial terms, the easy axes are at $\alpha_{1,2} = \pm(\pi/4 - \delta)$ and $\theta_{3,4} = \pm(3\pi/4 + \delta)$ with $\delta = 1/2\sin^{-1}(K_{u1}/4K_1)$. If the uniaxial anisotropy constant is negligible, $\delta = 0$ and the easy axes directions are at $\alpha = \pm\pi/4, \pm 3\pi/4$, as expected from bi-axial anisotropy. As the uniaxial anisotropy constant increases, δ increases and the angle between the easy axes that are bisected by the uniaxial anisotropy is smaller.

1.1.4 Magnetization Switching

When an external magnetic field is applied to a sample, another term is added to the free energy equation: The Zeeman energy, $F = -\mu_m \cdot \mathbf{H}$, which is the potential energy of one magnetic moment in a magnetic field. For a bulk sample, the potential energy per unit volume is:

$$u_{Zeeman} = -\mathbf{M}\cdot\mathbf{H} \tag{1.4}$$

If the field is applied on a two-dimensional sample with bi-axial anisotropy with easy axes along the $\langle 1,1,0\rangle$ directions, the total free energy is:

$$E = K_0 + K_1 \cos^2 2\alpha - \mathbf{MH}\cos(\alpha - \beta) \tag{1.5}$$

where K_1 is the bi-axial anisotropy constant, α is the angle between $\mathbf{M}$ and the crystal axis [100], and β is the angle between $\mathbf{H}$ and the crystal axis [100]. The first term minimizes at $\alpha = \pm\pi/4, \pm 3\pi/4$, and is responsible for the easy axes along these directions. The second term minimizes when $\mathbf{M}$ is parallel to $\mathbf{H}$. The magnetization will orient in a direction that minimizes the free energy. This direction can be found using the conditions $\partial E/\partial\alpha = 0$ and $\partial^2 E/\partial\alpha^2 > 0$. When the magnetic field changes either its magnitude or orientation, the magnetization might orient in a position of a local minima which is not the global minima of the energy, because of a potential barrier that prevents it from pointing in the direction of the global minimum (the potential barrier is a local maximum of the free energy). If we do not take into account fluctuations caused by external sources (such as heat), the magnetization will move to the global minima only after the potential barrier is removed, by changing the external magnetic field. When the potential barrier is weak, a small change in the external applied magnetic field can cause the magnetization direction to change dramatically. This abrupt changes of the magnetization orientation following small changes in $\mathbf{H}$ are called magnetization switchings. Figure 1.1 illustrates the energy plots of a sample with bi-axial anisotropy and a magnetic field of several amplitudes.

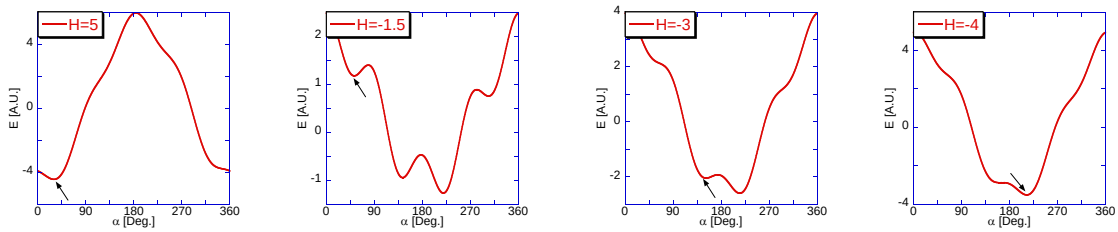

Figure 1.1: The energy given in Eq. 1.5 as a function of α. The applied magnetic field is oriented at $\beta = 10°$, with magnitude changing from positive to negative (arbitrary units). In this simulation, both $K_1 = 1$ and $|\mathbf{M}| = \mathbf{1}$. The arrow indicates the energy minimum in which the magnetization is found. From left to right: (H=5) When **H** is large, there is only one minimum and the magnetization points between the easy axis at $\alpha = 45°$ and the magnetic field. (H=-1.5) As the field decreases and becomes negative, the hard axis at $\alpha = 90°$ prevents the magnetization from pointing towards the global minimum, and it stays in the vicinity of the first easy axis at $\alpha = 45°$. (H=-3) As the magnetic field is further decreased, the potential barrier flattens, and the magnetization switches and points in the general direction of the easy axis at $\alpha = 135°$, another potential barrier is blocking the magnetization from pointing at the global minima. (H=-4) Finally, as the magnetic field is negative enough, the second potential barrier is removed and the magnetization points in an angle between the easy axis at $\alpha = 225°$ and the magnetic field.

1.2 Anisotropic Magnetoresistance and Planar Hall Effect

1.2.1 Physical Origin

Anisotropic magnetoresistance (AMR) in ferromagnetic materials is the dependance of the electrical resistivity on the angle between the current direction, **J**, and the magnetization orientation, **M**. The AMR is a spin-orbit effect, however, the specific mechanism is system dependent. For the itinerant ferromagnetic $3d$ alloys with the exchange split bands the AMR is commonly interpreted in the framework of Mott's two current model [1]. According to this model, below T_C, the spin direction of the charge carriers is conserved during most scattering events. Thus, the charge

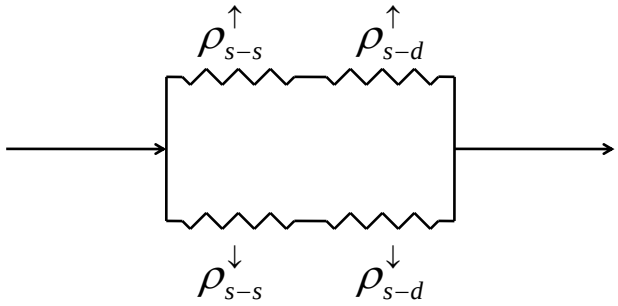

Figure 1.2: Resistor network representing the two-current model. The current is split between majority and minority electrons. The resistivity caused by scattering mechanisms for $s-s$ and $s-d$ scattering can be found separately and summed.

carriers having spin up and spin down can be represented as two parallel paths along which conduction can take place. A material in this model has two types of resistivity, represented as $\rho^{\uparrow}$ and $\rho^{\downarrow}$ which are not necessarily equal because of the difference in the density of spin-up and spin-down states at the Fermi energy (E_F). In addition, we note that the highest s band and the d band just below it (i.e., $4s$ and $3d$, $5s$ and $4d$, etc.) overlap. The majority of conductance is done by s electrons because of their lower effective mass. The s electrons can scatter into an unoccupied d state ($s-d$ scattering) or into another s state ($s-s$ scattering or "ordinary scattering"). However, $s-d$ scattering happens more often since the density of states for d electrons at the Fermi level is much greater than the corresponding density of states for s electrons.

Schematically, we can represent these independent spin channels resistivity in the resistor network shown in Figure 1.2. The channel resistivities can be added in parallel in order to obtain the overall resistivity.

The AMR yields a transverse "Hall like" field if $\mathbf{J}$ is neither parallel nor perpen-

dicular to **M**. This effect is called the "planar Hall effect" [2] since it produces a Hall voltage while having all of the relevant vectors in the plane of the film.

1.2.2 Mathematical Analysis

We now turn to formulate a set of equations which present the longitudinal and transverse resistivities for isotropic materials. The relation between the electric field and the current density is given by Ohm's law [3]:

$$\mathbf{E} = \rho \mathbf{J} \tag{1.6}$$

In the general two dimensional case, ρ is a tensor, and for a material that exhibits AMR it is given by:

$$\rho = \begin{pmatrix} \rho_{\parallel} & \\ & \rho_{\perp} \end{pmatrix}, \tag{1.7}$$

where $\rho_{\parallel}$ and $\rho_{\perp}$ are the resistivities for the currents parallel and perpendicular to the magnetization, respectively. We now define $\hat{u} = \langle \cos\varphi, \sin\varphi \rangle$, a unit vector in the direction of the current **J**, where φ is the angle between **J** and **M**. The longitudinal resistivity, measured in the **J** direction, is given by:

$$\rho_{long} = \frac{\mathbf{E} \cdot \hat{\mathbf{u}}}{|\mathbf{J}|} \tag{1.8}$$

By substituting equation 1.6 into equation 1.8 we obtain:

$$\rho_{long} = \frac{\hat{u}\rho\mathbf{J}}{|\mathbf{J}|} = \hat{u}\rho\hat{u}^T \tag{1.9}$$

and finally:

$$\rho_{long} = \rho_{\perp} + \left(\rho_{\parallel} - \rho_{\perp}\right)\cos^2\varphi \tag{1.10}$$

which is the longitudinal resistivity, denoted as AMR, measured along the **J** direction for a material exhibiting anisotropic magnetoresistance.

By defining a unit vector perpendicular to the current direction, $\hat{v} = \langle -\sin\varphi, \cos\varphi \rangle$, we can extract the transverse resistivity:

$$\rho_{trans} = \frac{\mathbf{E} \cdot \hat{\mathbf{v}}}{|\mathbf{J}|} \tag{1.11}$$

which always exists when the current direction is neither parallel nor perpendicular to the magnetization in a material exhibiting AMR. Substituting equation 1.6 in equation 1.11 yields:

$$\rho_{trans} = \frac{\hat{v}\rho\mathbf{J}}{|\mathbf{J}|} = \hat{v}\rho\hat{u}^T \tag{1.12}$$

and finally:

$$\rho_{trans} = \left(\rho_\perp - \rho_\parallel\right) \sin\varphi \cos\varphi \tag{1.13}$$

This transverse resistivity is called the planar Hall effect (PHE).

The PHE is *symmetric* under magnetization inversion. Therefore, the PHE is most apparent when $\mathbf{M}$ changes its orientation axis - preferably between $\varphi = 45°$ and $\varphi = 135°$.

The PHE in magnetic materials has been used so far mainly in $3d$ ferromagnetic layers and multilayers as a tool for measuring in-plane magnetization [4, 5, 6, 7, 8]. In addition there have also been suggestions to use it for low-field magnetic sensors [9].

1.2.3 Giant Planar Hall Effect

A dramatic development related to the PHE occurred recently with the discovery of the giant planar Hall effect (GPHE) in epitaxial films of the magnetic semiconductor (Ga, Mn)As by the groups of Awschalom (Santa Barbara) and Roukes (Caltech) [10] (see also the report in *Nature Materials* [11]). The two groups found that the

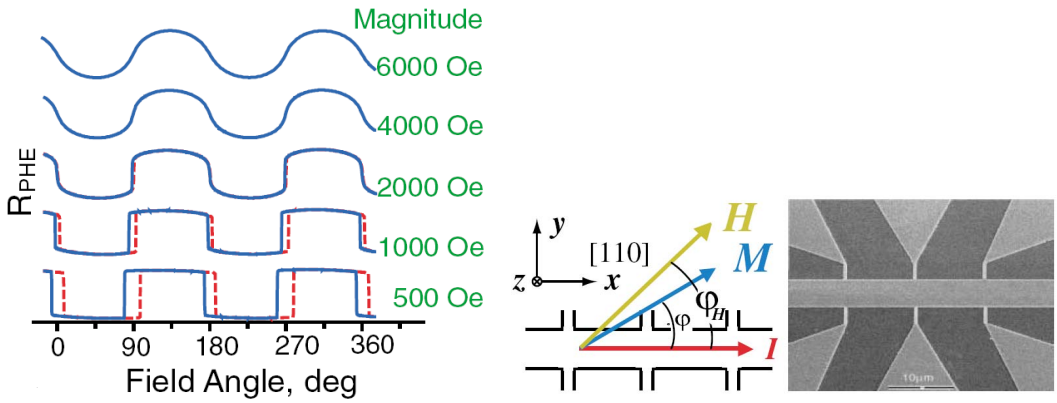

Figure 1.3: Figure from [10]. Right: The patterned Ga(Mn)As film with current path in the [110] direction. Left: the PHE in field orientation sweeps for different field magnitudes. The field angle is relative to the current path.

PHE in (Ga, Mn)As is orders of magnitude larger than in previously measured ferromagnetic metals, and thus named it with the prefix "giant", and also that it is manifested in striking switching behavior.

Figure 1.3 shows the planar Hall effect in (Ga, Mn)As as a function of the angle between the applied field and the current. For high fields the induced magnetization follows the applied field direction and thus the expected angular dependence given in Eq. 1.10 is obtained. For lower fields the underlying bi-axial magnetocrystalline anisotropy with easy axes along [100] and [010] is manifested by the sticking of the magnetization along a specific direction until it "jumps" to the other easy axis. Shortly afterwards we reported that GPHE is also found in manganite films [12]. The film we used was a 40-nm thick $La_{1-x}Sr_xMnO_3$ (LSMO) with a doping level of x=0.16. Figure 1.4 shows the transverse resistivity and longitudinal resistivity of the LSMO film as a function of the angle φ between the field applied in the film plane and the current while the magnitude of the field is kept constant. For high fields the

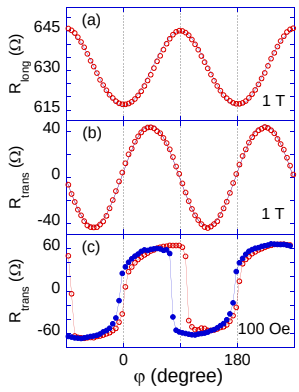

Figure 1.4: Measurements of longitudinal R_{long} and transverse R_{trans} signals of an $La_{0.84}Sr_{0.16}MnO_3$ film vs. φ (the angle between $\mathbf{M}$ and $\mathbf{J}$) at $T = 120$ K. (a) R_{long} vs. φ with H = 1 T. The line is a fit to Eq. 1.10. (b) R_{trans} vs. φ with H = 1 T. The line is a fit to Eq. 1.13. (c) R_{trans} vs φ with H = 0.01 T with clock-wise (full symbols) and anti-clock-wise (empty symbols) rotations.

magnetization is assumed to follow the applied field and the longitudinal resistivity indicates AMR behavior following $\cos^2\varphi$ dependence while the transverse resistivity is fit with $\sin\varphi\cos\varphi$ dependence, as expected from equations 1.10 and 1.13.

Similar to the behavior observed in GaMn(As), at lower fields the angular dependence changes as the effect of the sample magnetocrystalline anisotropy becomes noticeable, and sharp switches in the PHE are observed. We interpret the switches as jumps between two easy axes and since the symmetry axes for the switchings are $\varphi = 0°$ and $\varphi = 90°$ it is reasonable that the easy axes are in between; namely, at $\varphi_1 = 45°$ and $\varphi_2 = 135°$. This may not be exact, however, in view of the different hysteresis around $\varphi = 0°$ and $\varphi = 90°$ which could indicate that the two easy axes are not strictly perpendicular but are at $\varphi_1 = 45° + \delta\alpha$ and $\varphi_2 = 135° - \delta\alpha$. If $\delta\alpha > 0$ this would mean that for the symmetry axis at $\varphi = 0°$ the two easy axes are farther away than for the symmetry axis at $\varphi = 90°$. Two perpendicular easy axes

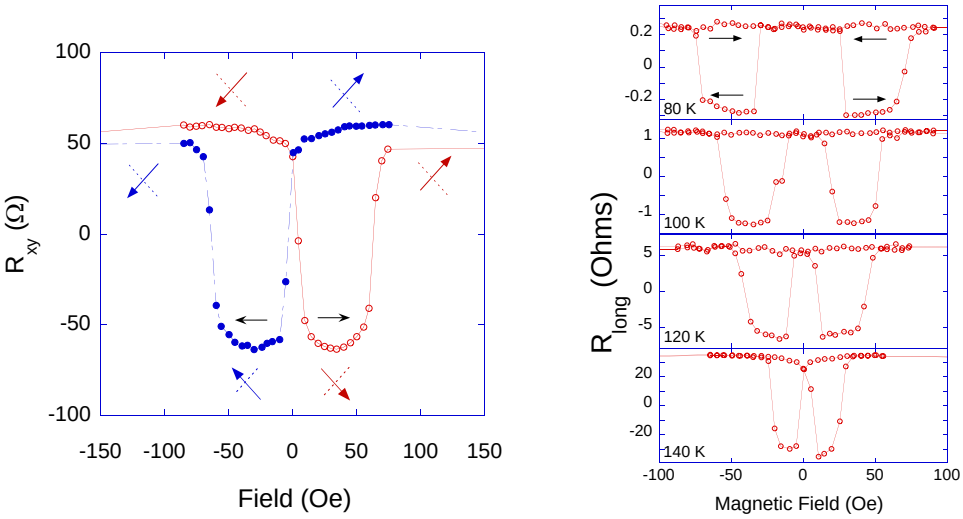

Figure 1.5: Left: The PHE vs. H at T = 120 K with $\beta = 10°$. The arrows indicate the magnetization orientation along EA1 or EA2 while the dashed line indicates the other easy axis. Right: PHE vs. H using a different pattern with $\beta = 10°$ at several temperatures. The parallel arrows, in both figures, indicate the field-sweep direction.

with different anisotropy would cause a difference between clock-wise field rotations and counter-clock-wise field rotations but not in the overall hysteresis around the two symmetry axes.

1.2.4 Planar Hall effect switching

As mentioned before, the magnetocrystalline anisotropy gives rise to the switching behavior of the magnetization. Since the PHE depends on the magnetization orientation, the switching is also observed in a transport measurement of the PHE signal. Figure 1.5 shows the PHE of LSMO with doping level of x=0.16, with current path along the [100], and the angle between the field and the current is kept constant while the field is swept: At high fields the magnetization is parallel to the applied field. As the field is decreased, the magnetization aligns along the closer easy axis, and then,

as the field is reversed, it switches to the other easy axis and then back to the initial easy axis. Each jump between the easy axes oriented at $\varphi = 45°$ and $\varphi = 135°$ is accompanied by a sign reversal in the PHE.

The switching behavior is particularly interesting because it is similar to that observed in GMR heterostructures [13] and in ferromagnetic tunnel junctions [14] (see Figure 1.6) that have an important place in the emerging field of spin selective electronics known as "spintronics" or magneto-electronics [15] (spintronics, GMR, and TMR are explained in more details in section 1.3). We note that the GPHE found in the magnetic semiconductor appears only below 50 K and half of its magnitude is lost already at $T \sim 5\ K$. The GPHE found in LSMO with a doping level of x=0.16 is of comparable magnitude, but persists to much higher temperatures (up to $\sim 140\ K$, see figure 1.7). Higher doped manganites allowed us to achieve GPHE behavior even above room temperature.

The temperature dependence of the switching shows that the jumps rapidly decrease as a function of temperature. Based on measurements as shown in Figure 1.4 and Equations 1.10 and 1.13 we calculate at different temperatures $\Delta\rho = \rho_{\parallel} - \rho_{\perp}$ which is the maximum possible jump. Figure 1.7 shows $\Delta\rho$ as extracted from AMR measurements ($\Delta\rho_{AMR}$), $\Delta\rho$ as extracted from PHE measurements ($\Delta\rho_{PHE}$), and $\Delta\rho$ as extracted from the measured jump in field sweeps ($\Delta\rho_{jump}$). Clearly the three quantities exhibit similar temperature dependence while changing by more than two orders of magnitude. We see, however, that there is a significant difference between $\Delta\rho_{AMR}$ and $\Delta\rho_{PHE}$. This discrepancy will be addressed in the next section.

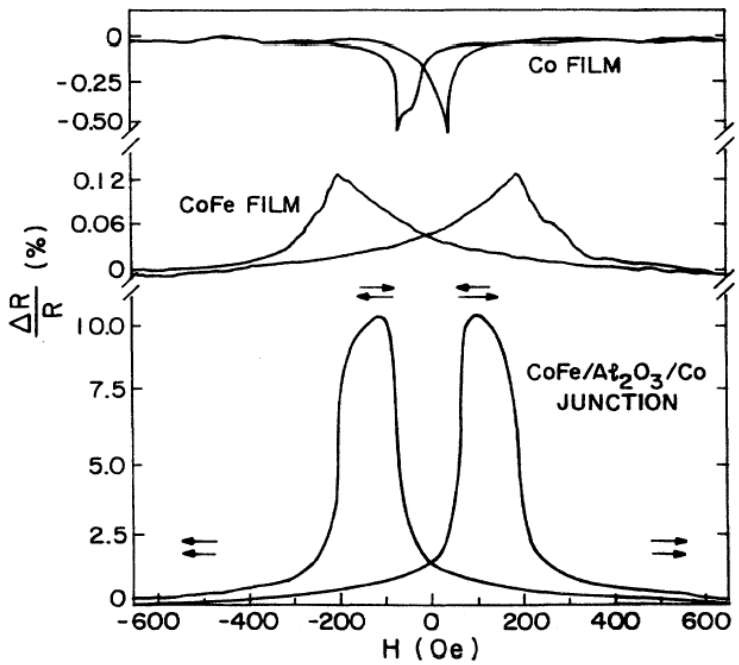

Figure 1.6: Figure from [14]. Resistance of CoFe/Al_2O_3/Co junction plotted as a function of H in the film plane, at 295 K. Also shown is the variation in the CoFe and Co film resistance. The arrows indicate the direction of M in the two films.

1.2.5 Higher order Equations

Since equations 1.10 and 1.13 consider only the angle between **J** and **M** and ignore their orientation relative to crystal axes, they are expected to strictly apply only to amorphous magnetic films and not to magnetic crystals [16]. Surprisingly, these equations appear to describe AMR and PHE in various epitaxial magnetic films [10, 17, 18], including manganites [19], at least qualitatively, despite some quantitative discrepancies that have been observed and attributed to extrinsic effects. As mentioned before, the term $(\rho_{\parallel} - \rho_{\perp})$ in Eq. 1.10 differed from $(\rho_{\parallel} - \rho_{\perp})$ in Eq. 1.13 (See Figure 1.4, for example, where the amplitudes of the PHE and AMR signals are different). Moreover, low temperature AMR measurements cannot be fitted with a

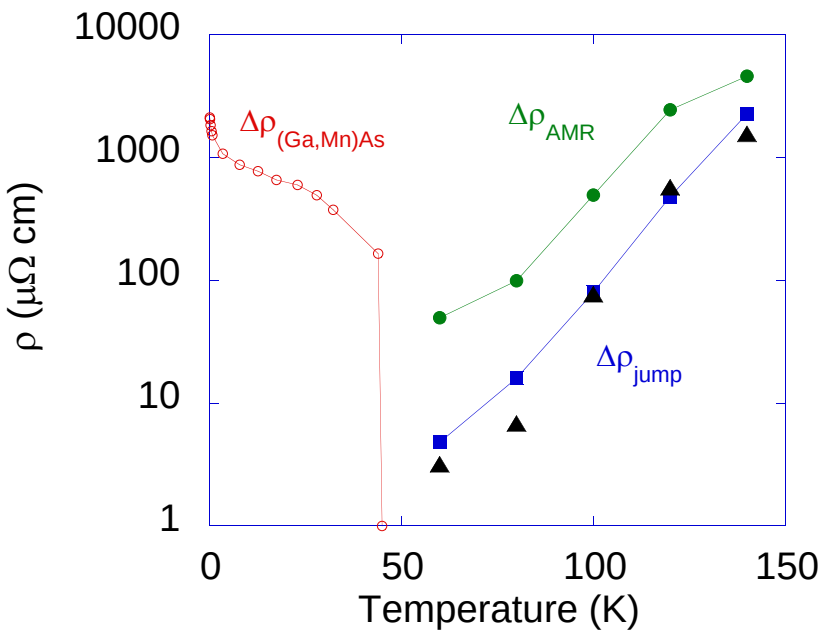

Figure 1.7: $\Delta\rho_{AMR}$ (connected circles), $\Delta\rho_{PHE}$ (unconnected triangles) and $\Delta\rho_{jump}$ (connected squares) of LSMO with x=0.16 vs T. $\Delta\rho_{jump}$ in (Ga, Mn)As calculated based on data extracted from [10], is given for comparison.

sinusoidal curve at all.

To obtain clear indication of crystal symmetry effects on the AMR and PHE of epitaxial films of manganites (LSMO and LCMO), we have used patterns with current paths at different angles θ relative to crystal axes and found a strong dependence of AMR and PHE on current direction; namely, a direct manifestation of crystal symmetry contribution. Here we concentrate on the determination of the 4th order resistivity tensor that fully describes the magnetotransport properties of the manganites studied.

As the experimental data clearly indicates that crystal contributions should be taken into consideration, we turn now to determine the resistivity tensor that will allow us to formulate AMR and PHE equations that will take into account both α

(the angle between **M** and $\langle 100 \rangle$) and θ (the angle between **J** and $\langle 100 \rangle$).

The resistivity tensor in a magnetic conductor depends on the direction cosines of the magnetization vector, α_i, and can be expressed as a series expansion of powers of the α_i, giving [20]:

$$\rho_{ij}(\alpha) = \sum_{k,l,m...=1}^{3} (a_{ij} + a_{kij}\alpha_k + a_{klij}\alpha_k\alpha_l + a_{klmij}\alpha_k\alpha_l\alpha_m + a_{klmnij}\alpha_k\alpha_l\alpha_m\alpha_n + ...) \quad (1.14)$$

where $i, j = 1, 2, 3$ and the a's are the expansion coefficients. As usual $\rho_{ij}(\alpha) = \rho^s_{ij}(\alpha) + \rho^a_{ij}(\alpha)$ where ρ^s_{ij} and ρ^a_{ij} are symmetric and antisymmetric tensors, respectively. The symmetric tensor ρ^s_{ij} is even in α_i:

$$\rho^s_{ij}(\alpha) = \sum_{k,l,m...=1}^{3} (a_{ij} + a_{klij}\alpha_k\alpha_l + a_{klmnij}\alpha_k\alpha_l\alpha_m\alpha_n + ...) \quad (1.15)$$

while ρ^a_{ij} is odd in α_i:

$$\rho^a_{ij} = \sum_{k,l,m...=1}^{3} (a_{kij}\alpha_k + a_{klmij}\alpha_k\alpha_l\alpha_m + ...). \quad (1.16)$$

As both AMR and PHE are symmetric, we use only ρ^s_{ij} for their expression. The manganite samples we measured are epitaxial films grown on a cubic substrate ($SrTiO_3$). In addition, they exhibit cubic bi-axial magnetic anisotropy in the film plane with easy axes in the $\langle 110 \rangle$ directions; therefore, as we are interested only in in-plane properties, we use the tensor expansion for crystals with m3m cubic-crystal structure [21]. The symmetric resistivity tensor for this class of materials up to the 4th order is given by:

$$\rho^s = \begin{pmatrix} C' + C'_1\alpha_1^2 + C'_2\alpha_1^4 + C'_3\alpha_2^2\alpha_3^2 & C'_4\alpha_1\alpha_2 + C'_5\alpha_1\alpha_2\alpha_3^2 & C'_4\alpha_1\alpha_3 + C'_5\alpha_1\alpha_3\alpha_2^2 \\ C'_4\alpha_1\alpha_2 + C'_5\alpha_1\alpha_2\alpha_3^2 & C' + C'_1\alpha_2^2 + C'_2\alpha_2^4 + C'_3\alpha_3^2\alpha_2^2 & C'_4\alpha_2\alpha_3 + C'_5\alpha_2\alpha_3\alpha_1^2 \\ C'_4\alpha_1\alpha_3 + C'_5\alpha_1\alpha_3\alpha_2^2 & C'_4\alpha_3\alpha_2 + C'_5\alpha_3\alpha_2\alpha_1^2 & C' + C'_1\alpha_3^2 + C'_2\alpha_3^4 + C'_3\alpha_1^2\alpha_2^2 \end{pmatrix}. \quad (1.17)$$

Since **M**, **J**, and the measurements are all in the film plane we use only the top left 2x2 terms of the ρ^s tensor, and set α_3 to zero. This leaves us with:

$$\rho^s = \begin{pmatrix} C' + C'_1\alpha_1^2 + C'_2\alpha_1^4 & C'_4\alpha_1\alpha_2 \\ C'_4\alpha_1\alpha_2 & C' + C'_1\alpha_2^2 + C'_2\alpha_2^4 \end{pmatrix} \tag{1.18}$$

Using the same calculation as in section 1.2, we define $\hat{u}$ and $\hat{v}$ as unit vectors parallel and perpendicular to **J**, respectively. The longitudinal resistivity measured along the **J** direction is given by $\rho_{long} = \frac{\bar{E}\cdot\hat{u}}{|J|}$ and the transverse resistivity measured perpendicular to **J** is given by $\rho_{trans} = \frac{\bar{E}\cdot\hat{v}}{|J|}$. Since $\bar{E} = \rho^s\bar{J}$ we obtain for the longitudinal resistivity $\rho_{long} = \frac{\hat{u}\rho^s\bar{J}}{|J|} = \hat{u}\rho^s\hat{u}^T$ and for the transverse resistivity $\rho_{trans} = \frac{\hat{v}\rho^s\bar{J}}{|J|} = \hat{v}\rho^s\hat{u}^T$ which gives new equations for describing AMR and PHE:

$$\rho_{long} = A\cos(2\alpha - 2\theta) + B\cos(2\alpha + 2\theta) + C\cos(4\alpha) + D \tag{1.19}$$

and

$$\rho_{trans} = A\sin(2\alpha - 2\theta) - B\sin(2\alpha + 2\theta), \tag{1.20}$$

where:

$A = \frac{C'_1}{4} + \frac{C'_2}{4} + \frac{C'_4}{4}$

$B = \frac{C'_1}{4} + \frac{C'_2}{4} - \frac{C'_4}{4}$

$C = \frac{C'_2}{8}$

$D = C' + \frac{C'_1}{2} + \frac{3c'_2}{8}$

Equations 1.19 and 1.20 are higher order equations which take into account the crystal symmetry. The parameter A is the coefficient of the term describing the non-crystalline contribution since $\alpha - \theta$ equals φ, the angle between **M** and the **J**. The parameters B and C arise due to crystalline contribution. We note that Eq. 1.20 can

be written as:

$$\rho_{trans} = E\sin(2\alpha - \phi_{trans}), \tag{1.21}$$

where $E^2 = A^2 + B^2 - 2AB\cos(4\theta)$ and $\sin\phi_{trans} = \frac{A+B}{E}\sin(2\theta)$. Since E depends on the angle θ, the amplitude of the transverse curves changes as θ changes. Moreover, the amplitude is close to zero when $\cos(4\theta) = 1$; namely at $\theta = 0, \frac{\pi}{2}$. When C is negligible, similar treatment can be done for Eq. 1.19, which can be written as:

$$\rho_{long} = F\cos(2\alpha - \phi_{long}) + D, \tag{1.22}$$

where $F^2 = A^2 + B^2 + 2ABcos(4\theta)$ and $\sin\phi_{long} = \frac{A-B}{F}\sin(2\theta)$. As in the transverse case, F depends on the angle θ and the amplitude of the longitudinal signal equals zero when $\cos(4\theta) = -1$; namely at $\theta = \pm\frac{\pi}{4}$. Since Eq. 1.21 and Eq. 1.22 have the same qualitative behavior in the low C limit as equations 1.10 and 1.13, the experimental data may appear to fit equations 1.10 and 1.13. When C is large (as is the case at low temperature) the AMR signal strongly deviates from amorphous sinus dependence due to the term $\cos(4\alpha)$. This is particulary the case when $\theta = \frac{\pi}{4}$ and $A \sim B$ (as is the case in LSMO) as the first two terms in Eq. 1.19 cancel out and the $\cos(4\alpha)$ term dominates. Detailed information regarding this work can be found in [22].

1.3 Spintronics

Spin selective electronics, also known as spintronics or magneto-electronics [15], is a rapidly evolving field of research that exploits the spin and magnetic moment of electrons, together with their electric charge, to create a new generation of electronic devices.

1.3.1 Giant Magnetoresistance

The birth of spintronics is attributed to the discovery of "Giant Magnetoresistance" (GMR) in 1988 by two independent groups led by Albert Fert and Peter Grunberg [23, 24]. The group led by Albert Fert studied heterostructures of Fe/Cr and the group led by Grunberg studied heterostructures of Fe/Cr/Fe. In the multilayers, each ferromagnetic layer was separated by a non-magnetic layer. The GMR effect is measured when the magnetic orientation of one of the layers is switched by the application of a magnetic field. The researchers found that when the magnetization of the two layers is parallel the resistance is lower as compared to the anti-parallel configuration. Soon thereafter GMR became a technological reality [25].

In 2007, Albert Fert and Peter Grunberg received a Nobel Prize in Physics for their discovery of the GMR.

1.3.2 Tunneling Magnetoresistance

An effect similar to the GMR is observed when the two ferromagnetic layers are separated by an insulating layer. In this case the effect is called tunneling magnetoresistance (TMR) and the structure itself is termed magnetic tunnel junction (MTJ)[14, 26]. A MTJ structure consists of two ferromagnetic layers separated by a thin, electrically insulating, tunnel barrier layer. The tunnel barrier layer is sufficiently thin to allow quantum tunneling of charge carriers between the ferromagnetic layers. The tunneling process is spin dependent, which means that the tunneling current across the junction depends on the relative orientation of the magnetization of the two ferromagnetic layers. Current MTJ structures can achieve $\sim$ 200

percent resistance differences between the parallel and antiparallel magnetization configurations[27, 28]. Since the late 1990's, GMR and TMR based devices have been incorporated into magnetic disk drives as read-heads. The high sensitivity of the new read-heads enabled meaningful increases in the data density on magnetic disks.

1.3.3 Magnetic Random Access Memory

Random-access memory (RAM) is a form of digital data storage. It allows the stored data to be accessed in any order (i.e., at random). The word random thus refers to the fact that any piece of data can be recovered in a constant time, regardless of its physical location and whether or not it is related to the previous piece of data. This contrasts with storage mechanisms such as tapes, magnetic discs and optical discs, which rely on the physical movement of the recording medium or a reading head. In these devices, the movement usually takes longer than the data transfer, and the retrieval time varies depending on the physical location of the next item.

The three most important commercial high-density memory technologies are static random access memory (SRAM), dynamic random access memory (DRAM), and FLASH memory. Each of these memory devices uses an electronic charge to store information and each has its own advantages and disadvantages. For example, SRAM which typically uses six MOSFET transistors to store each memory bit, has fast read and write speeds, but it is expensive, volatile, and requires a large cell area. DRAM typically stores each data bit in a separate capacitor. Since capacitors leak charge, the information eventually fades unless the capacitor charge is refreshed periodically (hence the prefix dynamic). It has a high memory density, but it is also volatile

and requires refreshing of the storage capacitor every few milliseconds. This refresh requirement increases the complexity of the control electronics. FLASH is the major nonvolatile memory device in use today. Typical FLASH memory devices use charges trapped in a floating oxide layer to store information. Drawbacks to FLASH include high voltage requirements and slow program and erase times. Also, FLASH memory has a poor write endurance of about $10^4 - 10^6$ cycles before memory failure. In addition, to maintain reasonable data retention, the thickness of the gate oxide has to stay above the threshold that allows electron tunneling. This thickness requirement severely restricts the scaling trends of FLASH memory.

Unlike the conventional RAM chip technologies where the data bit is stored as electric charge or current flow, a memory state in magnetic random access memory (MRAM) is not maintained by power, but rather by the direction of a magnetic moment vector. The magnetic moment is a physical property of ferromagnetic materials and it is stable at temperatures below the T_c. The direction of the magnetization moment can be correlated with binary "0" and "1" for digital applications. A memory cell based on the magnetization state of a material is potentially an "ideal" memory because it has the properties of nonvolatility, high speed, unlimited write endurance, and low cost.

In typical MRAM devices, storing data is accomplished by applying magnetic fields and causing a magnetic material in an MRAM cell to be magnetized into either of two possible memory states. Recalling data is accomplished by sensing the resistive state of the cell which depends on the magnetic state. The magnetic fields are created by passing currents through strip lines external to the magnetic structure or through

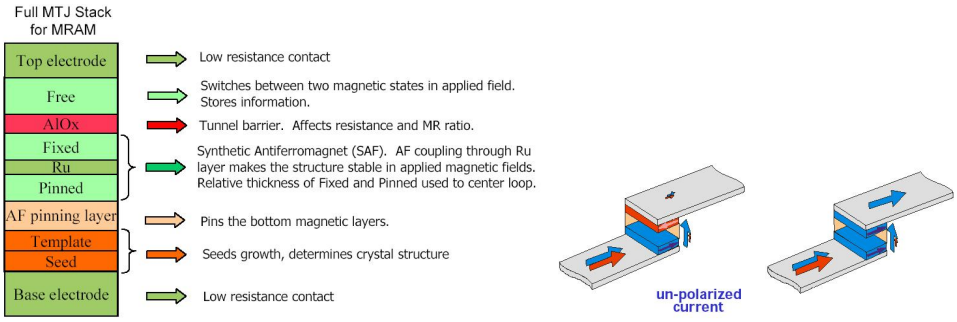

Figure 1.8: (Left)A sketch of a MTJ structure describing the plurality of layers required to obtain the TMR effect. (Right) MRAM memory cell based on the TMR effect, different orientation of the magnetic layer yields different resistance of the structure.

the magnetic structures themselves.

Early predecessors of modern MRAMs date from the 1960s when a magnetoresistive readout scheme was proposed for reading out the datum on a bit by detecting stray magnetic fields from the storage element. About 20 years later, a cell was proposed which used the magnetoresistance of the storage element itself to determine its memory state [29]. However, only a small fraction of the cell contributed to the readout signal. The birth of modern MRAM concepts took place at Honeywell in the mid-1980s. Cells first used AMR materials [30, 31] and then giant magnetoresistance [32] materials for data readout, and were fabricated with integrated circuits. These approaches did not result in components with competitive read access times, because the readout signal levels were small, until the invention of the pseudo-spin valve (PSV) [33, 34]. Current MRAM devices typically comprise a magnetoresistive tunneling junction (MTJ) [35, 36, 37].

One of the major drawbacks to the use of MTJ in MRAM devices and magnetic sensor devices is that MTJ's generally require a plurality of layers 1.8, which increases

the cost and complexity of forming such devices. Thus, it would be desirable to achieve the benefits realized by MTJ in a more straightforward and streamlined fashion.

1.3.4 GPHE based MRAM

Since the PHE signal depends on the angle of the magnetization relative to the current path (and the crystal axes), we can consider it as a tool to identify the magnetization orientation with a local transport measurement. Following this idea, we suggested the use of GPHE as the basis for a novel kind of MRAM. Magnetizing a film, which exhibit the GPHE, along $\varphi = 45°$ and $\varphi = 135°$ yields a PHE with opposite signs, according to Eq. 1.10. This can serve as the two states of a memory cell. If the material from which the device is made exhibits easy axes of magnetization along $\varphi = 45°$ and $\varphi = 135°$, it would be an advantage since it will make the two memory states more stable. Detailed description of this idea, along with demonstrations using both manganite and magnetite films can be found in [38] and [39]. This idea was also patented in [40].

Chapter 2

Materials

2.1 Manganites

The manganites are a very interesting material system that has attracted considerable theoretical and experimental interest in recent years. They present one of the central challenges in solid state physics since they are a strongly electron-correlated system with several competing ground states leading to the occurrence of charge ordering, orbital ordering, itinerant magnetism, insulating magnetism and phase separation [41].

2.1.1 Colossal Magnetoresistance

While the manganites were first mentioned in the fifties by Jonker and Van Santen [42, 43], who reported ferromagnetism in mixed crystals of $LaM^{3+}O_3 - MMn^{4+}O_3$, (M=Ca, Sr, or Ba), the current widespread interest in manganites started only in the early nineties, after a series of reports on large magnetoresistance effects in thin films of manganites: Kusters *et al.* [44] on $Nd_{0.5}Pb_{0.5}MnO_3$, von Helmolt *et al.* [45] on $La_{0.67}Ba_{0.33}MnO_3$ and Jin *et al.* [46] on $La_{0.67}Ca_{0.33}MnO_x$. Jin *et al.* reported a magnetoresistance ratio, defined as $\Delta R/R(H) = (R(0) - R(H))/R(H)$, with enormous

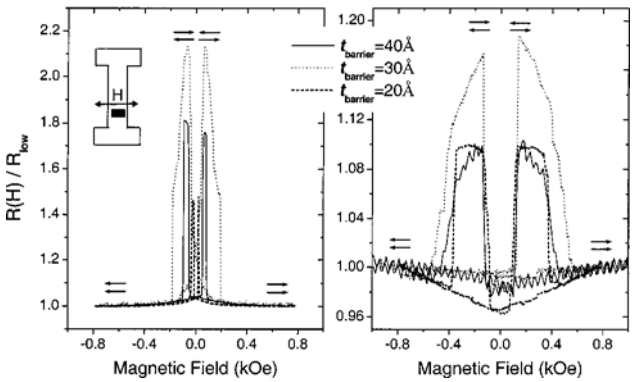

Figure 2.1: Figure from [47]. Resistance vs. magnetic field at 13 K of trilayer junctions ($La_{0.67}Sr_{0.33}MnO_3/SrTiO_3/La_{0.67}Sr_{0.33}MnO_3$) on $(LaAlO_3)_{0.3} - (Sr_2AlTaO_6)_{0.7}$ substrates (left) and on $NdGaO_3$ substrates (right), The inset shows the schematics of the geometry for the base stripe, the junction, and the direction of the applied field.

value of 1270 at T=77 K and H=6 T. Since this large magnetoresistance was much larger that the magnetoresistance ratio found in magnetic multilayered structures exhibiting giant magnetoresistance, the term colossal magnetoresistance (CMR) was used to describe this intriguing phenomenon.

Technologically, so far the CMR effect has not proven very useful due to the large fields (on the order of Tesla's) needed to obtain the colossal magnetoresistance. Therefore, there have been attempts to suggest tunnel junction structures with CMR materials [47] (see figure 2.1). These attempts, despite constant improvements, have not overcome so far the fast degradation of the junction with increased temperature. In this respect, the GPHE we found in manganites could be an alternative way of obtaining GMR-like functionality in manganites.

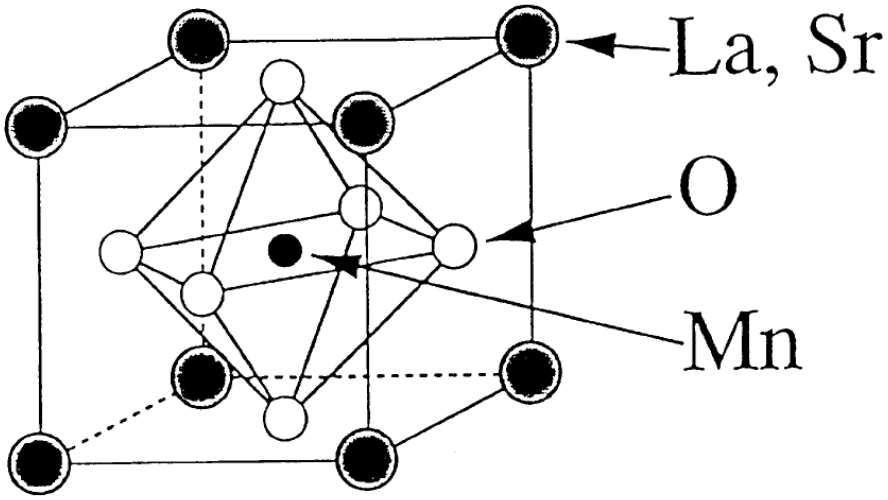

Figure 2.2: Arrangement of ions in the perovskite crystal structure of LSMO.

2.1.2 Crystal Structure

The manganites have perovskite crystal structure and share the chemical formula of $T_{1-x}D_xMnO_3$, where 'T' is a trivalent lanthanide like La, Pr, or Nd (with probability of $1 - x$) and 'D' is a divalent alkaline earth element like Ca, Sr, Ba (with probability of x). One can consider the manganites to have a FCC crystal structure with 'T' or 'D' ions at the corners, oxygen ions in the center of the face edges, and manganese ion in the middle of the cube. The perovskite lattice structure of these materials is illustrated for LSMO as an example in figure 2.2.

2.1.3 Phase Diagrams

The trivalent lanthanide and the divalent alkaline earth have a significant effect on the properties of the manganites, in particular through their effect on the bandwidth (as discussed below). During my research I focused on two families of manganites:

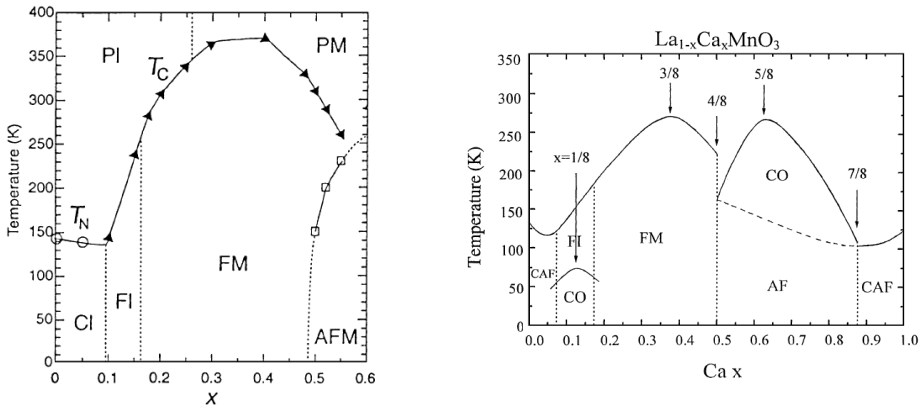

Figure 2.3: (Left): Phase diagram of $La_{1-x}Sr_xMnO_3$. T_n and T_c are the Neel and Curie temperatures, respectively. PI - paramagnetic insulator, PM - paramagnetic metal, CI - spin-canted insulator, FI - ferromagnetic insulator, FM - ferromagnetic metal, AFM - A-type antiferromagnetic metal. (Right) Phase diagram of $La_{1-x}Ca_xMnO_3$. FM - ferromagnetic metal, FI - ferromagnetic insulator, AF - antiferromagnetism, CAF - canted AF, and CO - charge/orbital ordering. FI and/or CAF could be a spatially inhomogeneous state with co-existing FM and AF.

$La_{1-x}Sr_xMnO_3$ - a wide bandwidth manganite, and $La_{1-x}Ca_xMnO_3$ - an intermediate bandwidth manganite. The differences in the properties of these manganites are shown in their phase diagrams presented in Figure 2.3.

2.1.4 Electronic State and Double Exchange Model

As mentioned above, the general form of the manganites is $T_{1-x}D_xMnO_3$, where 'T' is a trivalent lanthanide and 'D' is a divalent alakaline earth. The valency of the manganese depends on the value of x. Since the oxygen is in an O^{2-} state, it varies between Mn^{3+} for x=0 to Mn^{4+} for x=1. Consequently, Mn has either 3 or 4 valence electrons occupying the active $3d$ shell (we recall that neutral Mn has 7 electrons in the outer $3d$ shell). As shown in Figure 2.4, the 5 doubly degenerate 3d orbitals are split by the crystal field into two groups: 3 t_{2g} states and 2 e_g states. Deviations

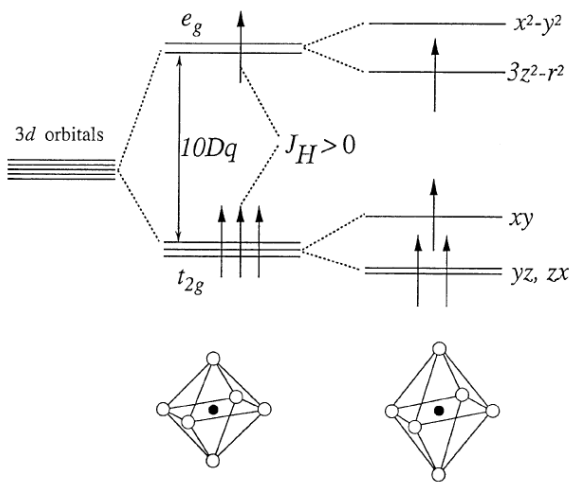

Figure 2.4: The 3d orbitals of Mn for a specific spin orientation are split by the cubic crystal field (10Dq) into 3 t_{2g} states and 2 e_g states. A Jahn-Teller distortion reduces the degeneracy. A positive Hund coupling (JH) favors parallel spin alignment. The configuration shown is for Mn^{3+}. In the Mn^{4+} the e_g state is unoccupied.

from perfect cubic structure reduce the degeneracy of these states. The energy of the t_{2g} states is lower, and large Hund coupling strongly favors parallel alignment of the electron spins; hence, in its Mn^{4+} state the three valence electrons occupy the 3 t_{2g} states, while in its Mn^{3+} state the fourth electron occupies the lower e_g state. The 3 parallel electrons occupying the 3 t_{2g} states are considered localized, and electrical transport occurs by the motion of the electron in the e_g state via the oxygen p orbitals.

Experimental observations show that while in the x=0 and x=1 states the manganites are insulating and antiferromagnetic, there is a range of doping where a ferromagnetic phase appears, which is correlated with the insulator to metal transition. As a result, suggestions were made regarding the origin of a ferromagnetic exchange that is not induced by regular super-exchange through the oxygen. The idea that was put forward by Zener [48, 49], and further developed by Anderson and Hasegawa

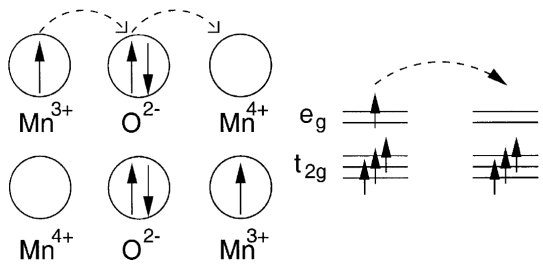

Figure 2.5: The double exchange process: an e_g electron hops between two neighboring Mn sites via two simultaneous motions in which one electron from the full oxygen shell hops to a Mn site with no e_g electrons and another e_g electron from a neighboring Mn site takes its place.

[50] and de Gennes [51], is based on the following assumptions: a) the interatomic exchange is strong, and therefore the only important configurations are those in which all spins of the 3d electrons in a specific Mn site are parallel - in particular, the spin of the electron occupying the e_g state is parallel to the s=3/2 spin of the 3 t_{2g} electrons; (b) carriers do not change their spin when they move; therefore, an e_g electron can hop to a neighboring site only if the spins of the t_{2g} electrons of the two neighboring Mn ions are not antiparallel; (c) the more mobile the charge carriers are, the lower the total energy of the system is. The conclusion from these assumptions is that the ferromagnetic order is induced by the energy gain obtained by making the electrons itinerant. This mechanism for ferromagnetism is called double-exchange since the hopping process of an e_g electron between 2 Mn sites is via two simultaneous motions of electrons. Figure 2.5 presents the double exchange process as considered by Zener [48]. A variation of this process, based on a second-order approximation, was subsequently considered by Anderson and Hasegawa [50].

2.2 Magnetite

Magnetite (Fe_3O_4) is one of the half metallic oxides most studied in recent years. It has an inverse spinel structure (see Figure 2.6) which means that instead of a structure of AB_2O_3, where A is a divalent ion and B is a trivalent ion, the trivalent ions occupy all the A sites and half of the B sites. Magnetite is ferrimagnetic [52, 53] with antiparallel coupling between A and B sites and Curie temperature of 858 K. The saturated magnetic moment is close to $4\mu_B$ per formula unit, which is expected, since the magnetic moments of Fe^{3+} in the A and B sites are mutually compensated and only moments of Fe^{2+} that has 4 aligned $3d$ electrons (Hund's rule) are contributing to the observed moment.

A feature that attracted considerable interest to magnetite for many decades is the Verwey transition at $T_V = 122\ K$ where the electrical conductivity drops sharply by two orders of magnitude upon cooling. This feature has been extensively studied over the years [54]. Recent works relate this phenomenon to crystal-structural transition from cubic metallic to distorted-cubic insulator [55, 56]. This feature has been also a useful indicator for the quality of magnetite samples since defects and off-stoichiometry smear the Verwey transition.

Potential spintronics application of magnetite shifted the interest from bulk samples to epitaxial films and their magnetoresistance properties were extensively studied [57, 58, 59, 60, 17]. It turns out that the properties of the films are highly sensitive to growing conditions such as: substrate, temperature, oxygen partial pressure, and film thickness. In addition, the fact that there are other stable iron oxides may introduce spurious phases. All this makes the growth of high quality epitaxial films of magnetite

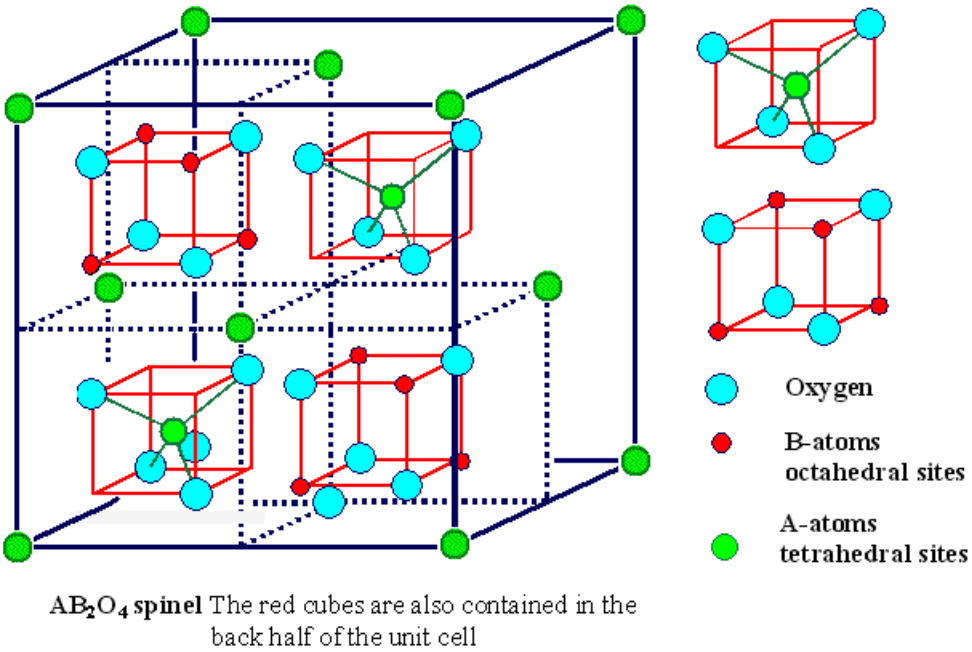

Figure 2.6: Spinel structure. Magnetite has an inverse spinel structure, meaning that the A sites are occupied by Fe^{3+} while the B sites are occupied half by Fe^{3+} and half by Fe^{2+}.

a considerable challenge.

Attempts to use the half metallicity of magnetite for enhanced spintronics devices were not very successful to date; in particular, TMR devices yielded a magnetoresistance effect which was much lower than expected, possibly due to spin flips at the interface with the insulating layer, or to the presence of a reduced oxide at this interface [61]. On the other hand, indications of very large planar Hall effect (PHE) may indicate a more promising way for using magnetite films in spintronic applications, as we presented in [39].

Chapter 3

Experimental details

3.1 Film Fabrication

All the films I measured during my Ph.D. were grown at Yale University by our collaborators, the group headed by Prof. Charles Ahn.

3.1.1 Manganites

The manganite films were deposited epitaxially on single-crystal $SrTiO_3$ substrates using off-axis magnetron sputtering. $\theta - 2\theta$ diffraction scan reveals c-axis (pseudo-cubic frame) oriented growth with a lattice constant of 0.383 nm. This spacing is consistent with a strained film [62, 63]. No other impurity phases are detected. Rocking curves taken around the 001 reflection have a typical full width at half maximum of 0.05 degrees. The surface roughness of the manganite layers has been analyzed using atomic force microscopy (AFM). The film surfaces have a root-mean-square (RMS) roughness of 0.2 nm. Samples consists of atomically flat terraces a few hundred angstroms wide separated by 0.4 nm high atomic steps. These terraces are due to the miscut in the $SrTiO_3$ single crystal substrate.

3.1.2 Magnetite

Magnetite samples were deposited by molecular beam epitaxy on a single-crystal MgO (100) substrate. Fe was evaporated from a high temperature effusion cell with an alumina crucible containing 99.995% pure Fe slugs. At the substrate temperature of 523 K, Fe was deposited with a rate of ~ 0.6 Å/sec and in oxygen excited by an ECR plasma source using an O_2 partial pressure of $2 \cdot 10^{-6}$ Torr. The quality of the sample was determined using surface characterization techniques (Reflection high energy electron diffraction (RHEED), low energy electron diffraction(LEED) and X-ray photoelectron spectroscopy (XPS)) and resistivity measurements, which exhibit a change in resistivity at the Verwey transition ($T_v = 122\ K$) of close to two orders of magnitude.

3.2 Sample Preparation

The films were patterned using photolithography to allow measurements of longitudinal and transverse signals. A typical pattern scheme is shown in Fig. 3.1. A photolithography process consists of several stages. First the film is coated with photoresist, which is a polymer sensitive to ultraviolet light. Second, ultraviolet light is shone through a mask onto the photoresist. Finally, the photoresist is developed, which selectively remove parts of it, transferring the pattern on the mask to the photoresist layer. There are two types of photoresist, termed positive and negative. A positive photoresist weakens when exposed to ultraviolet light, so when the sample is developed, parts that were covered by the mask will stay, creating a positive image of the mask on the sample. The opposite occurs with negative photoresist, which is

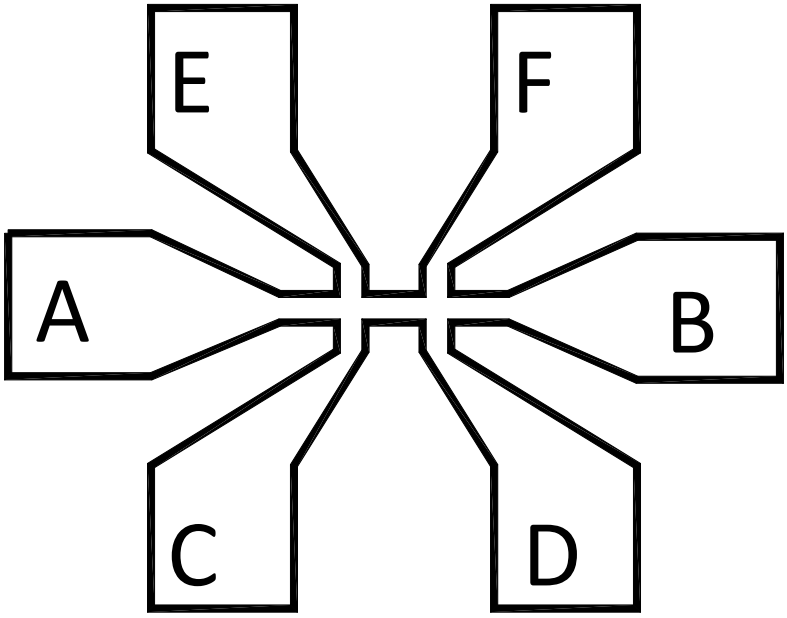

Figure 3.1: A typical pattern used for measurements. Current is flowing between terminals A and B. Longitudinal (AMR) measurement taken between C and D (or E and F). Transverse (PHE) measurements taken between C and E (or D and F).

strengthened while exposed to ultraviolet light, so by developing, a negative image of the mask is transferred to the sample. I used argon ion milling to remove the film where it is not covered by photoresist. Finally the resist is totaly removed by acetone leaving the patterned film ready for measurements. The preparation of manganite samples for measurement includes another lithography phase, this time in order to evaporate gold on the pattern contact pads. This is needed because of large contact resistance generated between LSMO and the aluminium wires used to connect the sample to the measuring instrument sample puck.

3.3 Equipment

Preparation and measurement equipment used in this work is briefly summarized here:

- Most transport measurements were carried using a Quantum Design Physical Property Measurement System (PPMS). The system includes a superconducting magnet capable of generating a magnetic field up to 9 T. Temperature can be controlled between $\sim 2\ K$ to 400 K. The magnetic field is aligned vertically, and two types of probes are available which allows rotation of the sample relative to the magnetic field with rotation axis either parallel or perpendicular to the field. The system uses the standard 4-probe measuring technique.

- Various Keithley instruments that were integrated into the PPMS environment enable us to enhance the measuring capability and flexibility of the PPMS. Improvements includes: Current source with greater power (up to 21 watts), a more sensitive voltmeter, a switch system that allows measurement of 6 channels at once (relative to 2 channels with the original PPMS system). The control software was written in C-sharp.

- Magnetization curves were taken using a Quantum Design Magnetic Properties Measurement System (MPMS), which employs SQUID (Superconducting QUantum Interference Device) technology. This system can generate magnetic field up to 7 T, and has the same temperature range as the PPMS, i.e., $\sim 2\ K$ to 400 K. Our system has both longitudinal and transverse magnetometer sensors, capable of measuring magnetic moments both parallel and perpendicular to the

applied magnetic field direction. The system is sensitive to magnetic moments down to $\sim 1^{-8}$ emu.

- A precision Etching Coating System (PECS) manufactured by Gatan. This system is used for etching samples that underwent photolithography and for sputtering, mainly of gold on the contact pads of samples.
- West Bond wire bonder, used to electrically attach samples to the sample holder of the measurement equipment. Aluminum or gold wires are available.
- A clean room with photolithography facilities.

3.4 Data Analysis

In this section I want to discuss the efforts needed in order to overcome experimental difficulties and achieve good fit of the raw data, especially to Eqs. 1.19 and 1.20. The majority of difficulties originates from misalignment of leads or smoothing of corners, which affect both AMR and PHE. Due to unavoidable misalignment of the pair of voltage leads when the transverse (PHE) resistance is measured, the longitudinal resistance also contributes to the measured values. The total resistance measured between terminals C and E for example, (Fig. 3.1) can be written as:

$$R_{CD} = R_{trans} + \epsilon R_{long} \tag{3.1}$$

where R_{trans} is the desired value, ϵ is proportional to the misalignment value, and R_{long} is the longitudinal (AMR) measurement taken between terminals C and D. We recall that according to Eq. 1.21, R_{trans} should have a sinusoidal behavior with mean value of zero. By using this condition with a fitting algorithm we can extract the value

of ϵ. This value is a geometric factor related to specific pattern, and should not change with temperature or magnetic field. The next step is converting the raw resistance data to resistivity. If we consider a sample of length l, width w, and thickness d, we note that:

$$\rho_{long} = \frac{E_{long}}{J_{long}} = \frac{V_{long}/l}{I/dw} \tag{3.2}$$

and

$$\rho_{trans} = \frac{E_{trans}}{J_{long}} = \frac{V_{trans}/w}{I/dw} \tag{3.3}$$

By substituting Ohm's law $V = IR$ in Eqs. 3.2 and 3.3, we obtain:

$$\rho_{long} = R_{long}\frac{dw}{l} \tag{3.4}$$

and

$$\rho_{trans} = R_{trans}d \tag{3.5}$$

Ideally, this conversion is simple since the geometry of the sample is known. However, as noted before, lithography variations might affect the length and width of the sample. We note that according to Eqs. 3.4 and 3.5, the transverse signal is less prone to lithography variations, since the thickness d is not affected by lithography. Therefore, we can convert PHE values to resistivity and fit the PHE values of all patterns first. Since the PHE signal (Eq. 1.20) depends only on A and B, at this point we do not have any knowledge of C and D. We now turn to the AMR curves. Firstly we need to normalize the length by dividing each value in each curve by the mean value of the specific curve, effectively making $D = 1$ for all curves. We expect that the fitting parameters for the AMR curves now will be: $A' = A/D$, $B' = B/D$, $C' = C/D$, and $D = 1$. We now fit all AMR curves with the restriction that the ratio of the

first 2 fitting parameters remains equal to the ratio we obtained from the PHE curves fitting, $A'/B' = A/B$. Now, we can extract D for each AMR curve by the simple calculation $D = A/A'$. By multiplying values of each AMR curve by the parameter D found for the specific curve, we obtain AMR curves of normalized length, which along with the unbiased PHE curves can be used by the fitting algorithm in order to extract all fitting parameters, A, B, C, and D.

Chapter 4

List of Publications

Giant planar Hall effect in colossal magnetoresistive $La_{0.84}Sr_{0.16}MnO_3$ **thin films**
Y. bason, L. Klein, J.-B. Yau, X. Hong, and C. H. Ahn, Applied Physics Letters **84**, 2593 (2004).

Characterization of the magnetic anisotropy in thin films of $La_{1-x}Sr_xMnO_3$ **using the planar Hall effect**
Y. Bason, L. Klein, J.-B. Yau, X. Hong, C. H. Ahn, Physica Status Solidi (c) **1**, No. 12, 3336-3338. (2004).

Planar Hall-effect magnetic random access memory
Y. Bason, L. Klein, J.-B. Yau, X. Hong, J. Hoffman and C. H. Ahn, Journal of Applied Physics **99**, 08R701 (2006).

Planar Hall effect in epitaxial thin films of magnetite
Y. Bason, L. Klein, H. Q. Wang, J. Hoffman, X. Hong, V. E. Henrich, and C. H. Ahn, Journal of Applied Physics **101**, 9J507 (2007).

The magnetoresistance tensor of $La_{0.8}Sr_{0.2}MnO_3$
Y. Bason, J. Hoffman, C. H. Ahn, and L. Klein, submitted to Physical Review B.

Chapter 5

Manuscripts

5.1 Giant planar Hall effect in colossal magnetoresistive $La_{0.84}Sr_{0.16}MnO_3$ thin films

HTML ABSTRACT + LINKS

Giant planar Hall effect in colossal magnetoresistive $La_{0.84}Sr_{0.16}MnO_3$ thin films

Y. Bason and L. Klein[a)]
Department of Physics, Bar Ilan University, Ramat Gan 52900, Israel

J.-B. Yau, X. Hong, and C. H. Ahn
Department of Applied Physics, Yale University, New Haven, Connecticut 06520-8284

(Received 2 December 2003; accepted 5 February 2004)

The transverse resistivity in thin films of $La_{0.84}Sr_{0.16}MnO_3$ (LSMO) exhibits sharp field-symmetric jumps below T_C. We show that a likely source of this behavior is the giant planar Hall effect combined with biaxial magnetic anisotropy. The effect is comparable in magnitude to that observed recently in the magnetic semiconductor Ga(Mn)As. It can be potentially used in applications such as magnetic sensors and nonvolatile memory devices. © *2004 American Institute of Physics.*
[DOI: 10.1063/1.1695197]

The planar Hall effect (PHE)[1] in magnetic conductors occurs when the resistivity depends on the angle between the current density **J** and the magnetization **M**, an effect known as anisotropic magnetoresistance (AMR).[2] When **M** makes an angle θ with **J**, the AMR effect is described by the expression $\rho=\rho_\perp+(\rho_\parallel-\rho_\perp)\cos^2\theta$, where $\rho_\perp$ and $\rho_\parallel$ are the resistivities for $\mathbf{J}\perp\mathbf{M}$ and $\mathbf{J}\parallel\mathbf{M}$, respectively. The AMR yields a transverse "Hall-like" field if **J** is not parallel or perpendicular to **M**. Assuming $\mathbf{J}=J_x\hat{x}$ and **M** are in the $x-y$ plane with an angle θ between them, the generated electric field has both a longitudinal component:

$$E_x=\rho_\perp j_x+(\rho_\parallel-\rho_\perp)j_x\cos^2\theta, \tag{1}$$

and a transverse component:

$$E_y=(\rho_\parallel-\rho_\perp)j_x\sin\theta\cos\theta. \tag{2}$$

This latter component is denoted the planar Hall effect. Unlike the ordinary and extraordinary Hall effects, the PHE shows an even response upon inversion of **B** and **M**; therefore, the PHE is most noticeable when **M** changes its axis of orientation, in particular between $\theta=45°$ and $\theta=135°$.

The PHE in magnetic materials has been previously investigated in $3d$ ferromagnetic metals, such as Fe, Co, and Ni films, as a tool to study in-plane magnetization.[3] It has also been studied for low-field magnetic sensor applications.[4] Recently, large resistance jumps in the PHE have been discovered in the magnetic semiconductor Ga(Mn)As below its Curie temperature, ~50 K.[5] Four orders of magnitude larger than what has been observed in ferromagnetic metals, it is called the giant planar Hall effect (GPHE). Ga(Mn)As exhibits biaxial magnetocrystalline anisotropy; consequently, the magnetization reversal in a field scan occurs in two steps of 90° rotations. When the current path lies between the two easy axes, the 90° rotations lead to switching-like behavior in the PHE, which is similar to the switching resistivity curves observed in giant magnetoresistance heterostructures[6] and tunneling magnetoresistance trilayers.[7] This suggests that the GPHE in magnetic materials may be suitable for applications in spintronics,[8] such as field sensors and nonvolatile memory elements.

Here we report on the GPHE observed in the colossal magnetoresistive material (CMR), $La_{1-x}Sr_xMnO_3$ (LSMO). When x is between 0.15 and 0.3, LSMO is a ferromagnetic metal at low temperatures and a paramagnetic insulator at high temperatures, with the Curie temperature coinciding with the metal–insulator transition temperature. Depending on the carrier concentration, the Curie temperature of LSMO ranges from 150 to 350 K. Here, we report on films with a doping level of $x\sim0.16$ and resistivity-peak temperature of ~180 K (see Fig. 1). The films exhibit transverse resistivity jumps comparable to that observed in Ga(Mn)As, and they persist up to temperatures >140 K.

Thin films (about 40 nm) of LSMO have been deposited epitaxially on single-crystal [001] $SrTiO_3$ substrates using off-axis magnetron sputtering. θ–2θ x-ray diffraction reveals c-axis oriented growth (in the pseudo-cubic frame), with a lattice constant of ~0.385 nm, consistent with a strained film.[9] No impurity phases are detected. Rocking curves taken around the 001 reflection have a typical full width at half maximum of 0.05°. The film surface has been characterized using atomic force microscopy, which shows a typical root-mean-square surface roughness of ~0.2 nm. The films are patterned into Hall bars using photolithography

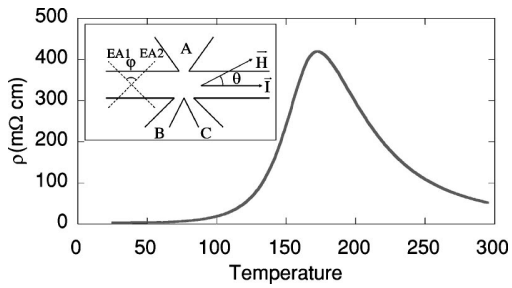

FIG. 1. ρ vs T for an LSMO thin film. Inset: The pattern used for resistivity and Hall measurements. The two easy axes directions (EA1 and EA2) and the angle (θ) between the applied field and the current are also shown. The current path is along either the [100] or [010] direction.

[a)]Electronic mail: kleinl@mail.biu.aci.il

 © 2004 American Institute of Physics
Downloaded 29 Jan 2009 to 132.70.50.117. Redistribution subject to AIP license or copyright; see http://apl.aip.org/apl/copyright.jsp

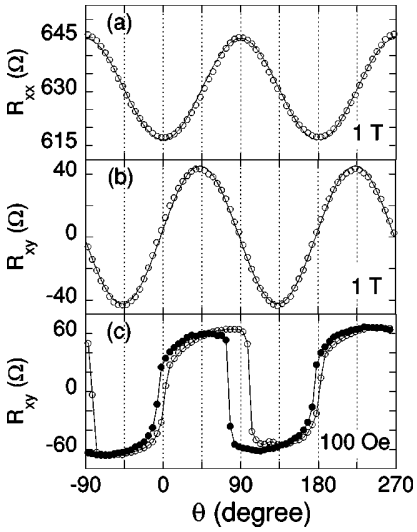

FIG. 2. Measurements of R_{xx} and R_{xy} vs θ at $T=120$ K. (a) R_{xx} measured between B and C. The line is a fit to $\cos^2\theta$. (b) R_{xy} measured between A and C. The line is a fit to $\sin\theta\cos\theta$. (c) R_{xy} measured between A and C with $H=100$ Oe.

for longitudinal and transverse resistivity measurements (see Fig. 1), with current paths along the [100] and [010] directions.

We first investigate the AMR in the LSMO films with a constant magnetic field applied in the plane of the film. Figure 2 shows the transverse resistivity and the longitudinal resistivity as a function of θ, the angle between the applied magnetic field and the current. The longitudinal resistance, R_{xx}, is measured between B and C (see Fig. 1). The transverse resistance, R_{xy}, is obtained by measuring the resistance between A and C and subtracting the longitudinal component based on the R_{xx} measurement. At high fields the magnetization is expected to be parallel to the applied field. We find that $R_{xx}(\theta)$ has a $\cos^2\theta$ dependence while $R_{xy}(\theta)$ has a $\sin\theta\cos\theta$ dependence. At lower fields, the angular dependence changes, as the effect of the magnetocrystalline anisotropy becomes significant, and we observe sharp switches in the PHE [see Fig. 2(c)]. We interpret the switches as jumps between easy axes; since the symmetry axes for the switchings are $\theta=0°$ and $\theta=90°$ it is reasonable that the easy axes are in between, namely at $\theta=45°$ and $\theta=135°$.

Figure 3 shows the switching behavior as a function of field sweeps with $\theta=10°$. At high positive field, the magnetization is parallel to the applied field, and the PHE is positive. As the field is reduced, the magnetization gradually aligns along the easy axis closer to the field orientation (EA2). As the field orientation is reversed, the magnetization first switches to the other easy axis (EA1), which is an intermediate state with a negative PHE. As the field becomes more negative, the magnetization goes back to the initial easy axis (EA2), but with opposite polarity. A similar process happens when the field is scanned from negative to positive field.

The temperature dependence of the switching shows that the jumps decrease rapidly as a function of temperature (Fig. 4). Based on the fits to the experimental data (as presented in Fig. 2) and Eqs. (1) and (2), we calculate $\Delta\rho=\rho_{\parallel}-\rho_{\perp}$ at different temperatures. Figure 4 shows $\Delta\rho$ extracted from

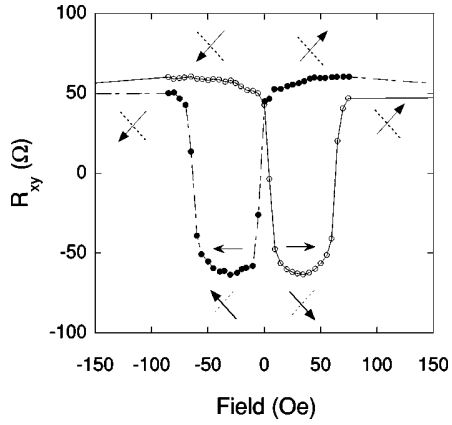

FIG. 3. PHE vs H at 120 K with $\theta=10°$. The arrow shows the magnetization direction along one of the easy axes while the dashed lines indicate the other easy axis direction. The horizontal arrows indicate the field sweep directions.

the AMR ($\Delta\rho_{\mathrm{AMR}}$), the PHE ($\Delta\rho_{\mathrm{PHE}}$) and the field sweep jump measurements ($\Delta\rho_{\mathrm{jump}}$) as a function of temperature. An in-plane magnetic field of 4 T was used to extract $\Delta\rho_{\mathrm{AMR}}$ and $\Delta\rho_{\mathrm{PHE}}$ at all temperatures. We see that $\Delta\rho_{\mathrm{AMR}}$ and $\Delta\rho_{\mathrm{PHE}}$ show similar temperature dependencies; however, there is a significant difference in their magnitude.[10] Considering possible sources for this difference, we note that Eqs. (1) and (2) are based on the assumption of uniform current, while the manganites are intrinsically inhomogeneous and exhibit percolative current paths.[11] In addition, these equations are expected to be valid for an isotropic medium. Here, the films are epitaxial and the role of crystal anisotropy is yet to be determined.

As shown in Fig. 4, the AMR and GPHE are also observed above T_C, and while switching is naturally not observed, the GPHE may still be interesting for applications where nonhysteretic behavior in field is required, such as Hall sensors.

Biaxial magnetic anisotropy in (001) LSMO films has previously been reported,[12] and there have been studies of biaxial anisotropy[13] and AMR[14] in other colossal magnetoresistance materials, such as $La_{1-x}Ca_xMnO_3$ (LCMO). Therefore, one may expect to observe the GPHE and switching behavior in CMR materials with other doping levels and chemical compositions.

In conclusion, we have observed the GPHE in LSMO thin films at temperatures as high as 140 K. By optimizing

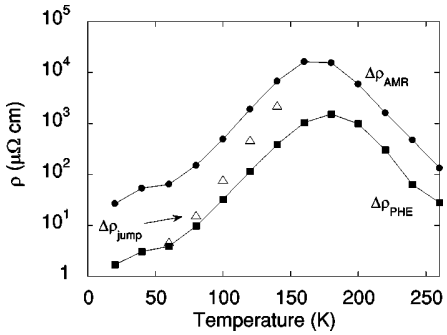

FIG. 4. $\Delta\rho_{\mathrm{AMR}}$ (connected circles), $\Delta\rho_{\mathrm{PHE}}$ (connected squares)—both measured in a 4 T field, and $\Delta\rho_{\mathrm{jump}}$ (unconnected triangles) vs T. $\Delta\rho_{\mathrm{jump}}$ is extracted at lower fields. The lines are guide to the eye.

Downloaded 29 Jan 2009 to 132.70.50.117. Redistribution subject to AIP license or copyright; see http://apl.aip.org/apl/copyright.jsp

the chemical composition and the device geometry, one may expect a larger effect at higher temperatures, thus allowing for the application of the GPHE in manganites, such as magnetic sensors and non-volatile memory devices.

L.K. and C.H.A. acknowledge support from Grant No. 2002384 from the United States–Israel Binational Science Foundation (BSF), Jerusalem, Israel. L.K. acknowledges support by the Israel Science Foundation founded by the Israel Academy of Sciences and Humanities. Work at Yale supported by AFOSR and NSF.

[1] C. Goldberg and R. E. Davis, Phys. Rev. **94**, 1121 (1954); F. G. West, J. Appl. Phys. **34**, 1171 (1963); W. M. Bullis, Phys. Rev. **109**, 292 (1958).
[2] T. R. McGuire and R. I. Potter, IEEE Trans. Magn. **11**, 1018 (1975).
[3] B. Zhao, X. Yan, and A. B. Pakhomov, J. Appl. Phys. **81**, 5527 (1997); A. Nemoto, Y. Otani, S. G. Kim, K. Fukamichi, O. Kitakami, and Y. Shimada, Appl. Phys. Lett. **74**, 4026 (1999); G. Li, T. Yang, Q. Hu, H. Jiang, and W. Lai, Phys. Rev. B **65**, 134421 (2002); Z. Q. Lu and G. Pan, Appl. Phys. Lett. **80**, 3156 (2002); S. Das, H. Yoshikawa, and S. Nakagawa, J. Appl. Phys. **93**, 8098 (2003).
[4] A. Schuhl, F. Nguyen Van Dau, and J. R. Childress, Appl. Phys. Lett. **66**, 2751 (1995).
[5] H. X. Tang, R. K. Kawakami, D. D. Awschalom, and M. L. Roukes, Phys. Rev. Lett. **90**, 107201 (2003).
[6] C. Vouille, A. Barthélémy, F. Elokan Mpondo, A. Fert, P. A. Schroeder, S. Y. Hsu, A. Reilly, and R. Loloee, Phys. Rev. B **60**, 6710 (1999).
[7] J. S. Moodera, L. R. Kinder, T. M. Wong, and R. Meservey, Phys. Rev. Lett. **74**, 3273 (1995).
[8] S. A. Wolf, D. D. Awschalom, R. A. Buhrman, J. M. Daughton, S. von Molnár, M. L. Roukes, A. Y. Chtchelkanova, and D. M. Treger, Science **294**, 1488 (2001).
[9] Y. Moritomo, A. Asamitsu, H. Kuwahara, and Y. Tokura, Nature (London) **380**, 141 (1996); H. W. Zandbergen, S. Freisem, T. Nojima, and J. Aarts, Phys. Rev. B **60**, 10259 (1999).
[10] The difference in the magnitude of $\Delta\rho_{\mathrm{AMR}}$ and $\Delta\rho_{\mathrm{PHE}}$ is also sample dependent.
[11] For a review see, e.g., E. Dagotto, T. Hotta, and A. Moreo, Phys. Rep. **344**, 1 (2001).
[12] L. M. Berndt, V. Balbarin, and Y. Suzuki, Appl. Phys. Lett. **77**, 2903 (2000).
[13] J. O'Donnell, M. Onellion, M. S. Rzchowski, J. N. Eckstein, and I. Bozovic, Phys. Rev. B **55**, 5873 (1997).
[14] J. O'Donnell, J. N. Eckstein, and M. S. Rzchowski, Appl. Phys. Lett. **76**, 218 (2000).

Downloaded 29 Jan 2009 to 132.70.50.117. Redistribution subject to AIP license or copyright; see http://apl.aip.org/apl/copyright.jsp

5.2 Characterization of the magnetic anisotropy in thin films of $La_{1-x}Sr_xMnO_3$ using the planar Hall effect

phys. stat. sol. (c) **1**, No. 12, 3336–3338 (2004) / **DOI** 10.1002/pssc.200405450

Characterization of the magnetic anisotropy in thin films of $La_{1-x}Sr_xMnO_3$ using the planar Hall effect

Y. Bason[*, 1], **L. Klein**[1], **J.-B. Yau**[2], **X. Hong**[2] and **C. H. Ahn**[2]

[1] Department of Physics, Bar Ilan University, Ramat Gan 52900, Israel
[2] Department of Applied Physics, Yale University, New Haven, Connecticut 06520-8284, USA

Received 27 June 2004, accepted 14 October 2004
Published online 20 December 2004

PACS 75.47.Gk, 75.47.Lx, 75.70.-i

Thin films of the colossal magnetoresistance material $La_{1-x}Sr_xMnO_3$ (LSMO) grown on $SrTiO_3$ substrates exhibit bi-axial magnetocrystalline anisotropy with easy axes along the [110] and [1$\bar{1}$0] directions. We have recently discovered that the intrinsic biaxial magnetic anisotropy combined with a giant planar Hall effect lead to striking switching behavior in the transverse resistivity of LSMO films (Appl. Phys. Lett. 84, 2593 (2004)). Here we use this phenomenon as a sensitive tool for measuring in-plane magnetization in order to characterize the magnetic anisotropy.

© 2004 WILEY-VCH Verlag GmbH & Co. KGaA, Weinheim

In an anisotropic conductor a current not flowing along one of the principal axes of the resistivity tensor is not parallel to the internal electric field. Thus, for a current path not along one of the principle axes, in addition to the longitudinal electric field, there is also a transverse electric field. In magnetic conductors, due to the dependence of the resistivity on the angle between the current and the magnetization (known as anisotropic magnetoresistance []) the in-plane principle axes of resistivity are parallel and perpendicular to the magnetization. Thus, for an angle θ between the current density **J** and the in-plane magnetization **M** with $\mathbf{J} = J_x\hat{x}$ and **M** in the $x - y$ plane, the generated electric field has both a longitudinal component: $E_x = \rho_\perp J_x + (\rho_\parallel - \rho_\perp)J_x \cos^2\theta$, and a transverse component: $E_y = (\rho_\parallel - \rho_\perp)J_x \sin\theta\cos\theta$ (where $\rho_\parallel$ and $\rho_\perp$ are the sensitivities for magnetization parallel to the current and magnetization perpendicular to the current, respectively) The latter term (E_y) is denoted the planar Hall effect.

In a recent work [] we have shown that the transverse resistivity in thin films of $La_{0.84}Sr_{0.16}MnO_3$ (LSMO) exhibits switching behavior whose origin is the intrinsic bi-axial magnetic anisotropy combined with giant planar Hall effect (GPHE). Here, we use the planar Hall effect for closer examination of the biaxial anisotropy itself.

Our samples are ~ 40 nm thick with $T_c \sim 180$ K. Details of sample preparation and characterization are given in [].

In our experiment, we apply a constant field in the film plane and the transverse resistivity is measured as a function of the field orientation as the field is swept clockwise and counterclockwise. Figure 1 shows the transverse resistivity and the longitudinal resistivity as a function of α, the angle between the applied magnetic field and the current. The current path is along either the [100] or [010] direction. At high fields the magnetization is parallel to the applied field. Consequently, the longitudinal resistivity (measured between B and C, see Figure 1) has a $\cos^2\theta$ dependence, while the transverse resistivity (measured between A and B with substraction of the longitudinal component) has a $\sin\theta\cos\theta$ dependence, as expected. At lower fields (see Figure 2), the manetocrystalline anisotropy becomes relevant and the orientation of the magnetization deviates from the field orientation towards the closest easy axis. Moreover, the angular dependence of **M** becomes discontinuous with jumps from the vicinity of one easy axis to the other which

* Corresponding author: e-mail: basony@mail.biu.ac.il, Tel.: 972-3-5317629, Fax: 972-3-5353298

© 2004 WILEY-VCH Verlag GmbH & Co. KGaA, Weinheim

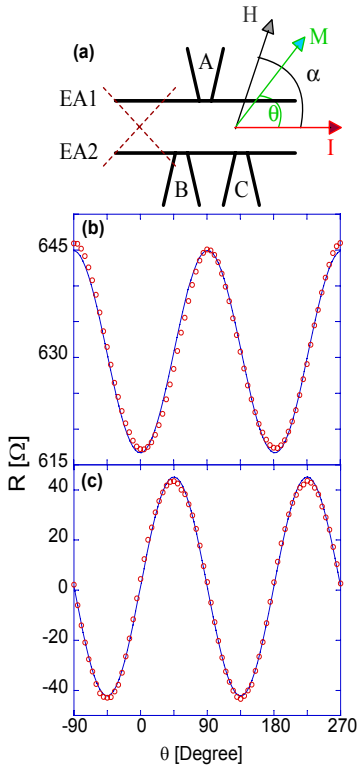

Fig. 1 (a) The pattern used for resistivity and Hall measurements. The two easy axes directions (EA1 and EA2) and the angle (α) between the applied field and the current are also shown. The current path is along either the [100] or [010] direction. (b) Longitudinal resistivity (measured between B and C) at T=120 K with H=1 T. The line is a fit to $\cos^2\theta$. (c) Transverse resistivity (measured between A and B). The line is a fit to $\sin\theta\cos\theta$.

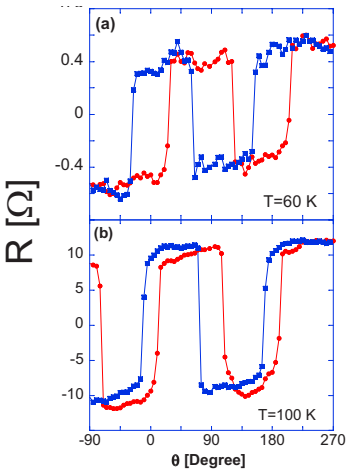

Fig. 2 Measurements of the transverse resistivity at H=100 Oe. (a) Transverse resistivity vs. θ at T=60 K. (b) Transverse resistivity vs. θ at T=100 K.

© 2004 WILEY-VCH Verlag GmbH & Co. KGaA, Weinheim

are manifested in the switching behavior of the transverse resistivity. As noted before in [], the switchings occur close to $\theta = 0°$ and $\theta = 90°$. Thus, to a first approximation, the easy axes point along $\theta \sim 45°$ and $\theta \sim 135°$; namely close to the [110] and [1$\bar{1}$0] directions.

In some cases, however, it is noticeable that the hysteresis resulting from clockwise and counter-clockwise rotations is different around the two easy axes. This suggests that the magnetocrystalline anisotropy is not strictly bi-axial.

The deviation from bi-axial anisotropy in our samples is similar to that observed in the magnetic semiconductor (Ga,Mn)As for which giant planar Hall effect was also reported []. For (Ga,Mn)As, the deviation was attributed to a weak uniaxial anisotropy superimposed along one of the cubic anisotropy hard axis. In this case, the free energy density is given by: $E = K_u \sin^2\theta + K_1/4\cos^2 2\theta - MHcos(\alpha - \theta)$. The first term (related to uniaxial anisotropy) minimizes at $\theta = 0$ and $\theta = \pi$, while the second term (related to bi-axial anisotropy) minimizes at $\theta = \pm 45°$ and $\theta = \pm 135°$. The third term, related to the magnetic potential, is isotropic. The equilibrium state can be found using the conditions $\partial E/\partial\theta = 0$ and $\partial^2 E/\partial\theta^2 > 0$. Due to the competition between the uniaxial and the bi-axial terms, the easy axes are at $\theta_{1,2} = \pm(\pi/4 - \delta)$ and $\theta_{3,4} = \pm(3\pi/4 + \delta)$ with $\delta = 1/2\sin^{-1}(K_u/K_1)$. Namely, the angle between the easy axes that are bisected by the uniaxial easy axis is smaller, hence, the hysteresis around the uniaxial axis is smaller.

Figure 2 presents the deviation from strict bi-axial anisotropy and it demonstrates that the deviation is less noticeable at lower temperatures. This suggests different temperature dependence for $\mathrm{K_u}$ and $\mathrm{K_1}$.

Acknowledgements L. K. and C. H. A. acknowledge support from Grant No. 2002384 from the United States-Israel Binational Science Foundation (BSF), Jerusalem, Israel. L.K. acknowledges support by the Israel Science Foundation founded by the Israel Academy of Sciences and Humanities. Work at Yale supported by AFOSR and NSF.

References

[1] T. R. McGuire and R. I. Potter, IEEE Trans. Magn. **11**, 1018 (1975).

[2] Y. Bason, L. Klein, J.-B. Yau, X. Hong, C. H. Ahn, et al., Appl. Phys. Lett. **84**, 2593 (2004).

[3] H. X. Tang, R. K. Kawakami, D. D. Awschalom, and M. L. Roukes, Phys. Rev. Lett. **90**, 107201 (2003).

© 2004 WILEY-VCH Verlag GmbH & Co. KGaA, Weinheim

5.3 Planar Hall-effect magnetic random access memory

Planar Hall-effect magnetic random access memory

Y. Bason[a] and L. Klein
Department of Physics, Bar Ilan University, Ramat Gan 52900, Israel

J.-B. Yau, X. Hong, J. Hoffman, and C. H. Ahn
Department of Applied Physics, Yale University, New Haven, Connecticut 06520-8284

(Presented on 3 November 2005; published online 18 April 2006)

We suggest a type of magnetic random access memory (MRAM) that is based on the phenomenon of the planar Hall effect (PHE) in magnetic films, and we demonstrate this idea with manganite films. The PHE-MRAM is structurally simpler than the currently developed MRAM that is based on magnetoresistance tunnel junctions, with the tunnel junction structure being replaced by a single-layer film. © *2006 American Institute of Physics*. [DOI: 10.1063/1.2162824]

Among various technologies considered for future memory applications, magnetic random access memory (MRAM) has attractive properties, since in addition to being nonvolatile with high endurance it can also be as fast as static random access memory (SRAM) and as dense as dynamic random access memory (DRAM).

Storing data in a typical MRAM device is accomplished by applying a magnetic field and causing a magnetic layer in the device to be magnetized in one of two possible states. Reading the data stored in a MRAM device requires reading the electrical resistance of the device, which depends on the magnetization orientation. Currently developed MRAM devices are based on magnetoresistance tunnel junctions[1,2] (MTJ), which are comprised of two ferromagnetic layers separated by a thin, electrically insulating tunnel barrier layer. The operative effect in MTJ structures exploits the asymmetry in the density of states of the majority and minority energy bands in a ferromagnet, with the tunneling resistance depending on the relative orientation of the magnetization vectors in the two magnetic layers. In the parallel configuration, there is a maximal match between the occupied states in one layer and the available states in the other layer, leading to a minimum in the tunneling resistance.

Current MTJ structures can achieve ~200% (Refs. 3 and 4) resistance differences between the parallel and antiparallel magnetization configurations, but these structures require a layering of numerous films and a relatively precise control of the thickness of the insulating layer. Also, in both states the measured voltage is of the same sign, so if MTJ structures are used in arrays, the variance of the voltages in the array must be much smaller than the difference in the average values of the distribution of the two states in the array.

We suggest here a different approach for storing a magnetic bit, which is based on the planar Hall effect (PHE).[5] The PHE in magnetic conductors occurs when the resistivity depends on the angle between the current density **J** and the magnetization **M**, an effect known as anisotropic magnetoresistance (AMR).[6] The AMR yields a transverse electric field when **J** is not parallel or perpendicular to **M**. If we assume **J** in the x direction and **M** in the $x-y$ plane with an angle θ between them, the generated electric field has both a longitudinal component,

$$E_x = \rho_\perp j_x + (\rho_\parallel - \rho_\perp) j_x \cos^2 \theta, \tag{1}$$

and a transverse component,

$$E_y = (\rho_\parallel - \rho_\perp) j_x \sin \theta \cos \theta. \tag{2}$$

The latter component is denoted the planar Hall effect. Unlike the ordinary and extraordinary Hall effects, the PHE shows an even response upon inversion of **J** and **M**. Therefore, the PHE is most noticeable when **M** changes its axis of orientation, in particular between $\theta=45°$ and $\theta=135°$. The PHE in magnetic materials has been previously investigated in 3d ferromagnetic metals, such as Fe, Co, and Ni films, as a tool to study in-plane magnetization.[7] It has also been studied for low-field magnetic sensor applications.[8] Recently, large resistance jumps in the PHE have been discovered in the magnetic semiconductor Ga(Mn)As below its Curie temperature, ~50 K. Four orders of magnitude larger than what has been observed in ferromagnetic metals, it has been termed the giant planar Hall effect (GPHE).[9] We previously reported that the GPHE can be observed in thin manganite films[10] at temperatures up to ~140 K. Here we show the PHE in manganite films above room temperature. In addition, we demonstrate the possible use of a thin manganite film as a memory cell operating at room temperature.

The samples we use are epitaxial thin films (~35 nm) of $La_{1-x}Sr_xMnO_3$ (LSMO), with $x=0.35$, and a resistivity peak temperature of ~390 K (see Fig. 1). The films are patterned for longitudinal and transverse resistivity measurements, with the current path along the [100] and [010] directions. Voltage sensing leads are connected perpendicular to the current path in a "Hall-like" configuration (see inset of Fig. 1). The "active area" (between C and D) on the current path is $2\times 2\ \mu m^2$.

Magnetizing the film along $\theta=45°$ and $\theta=135°$ yields a PHE with opposite signs, according to Eq. (2), which can serve as the two states of a memory cell. Figure 2 shows the PHE signal, R_{CD}, defined as the voltage between C and D divided by the current between A and B, while a field of 50 Oe is applied and then removed along $\theta=45°$ and $\theta=135°$, at

[a]Electronic mail: basony@mail.biu.ac.il

 © 2006 American Institute of Physics

Downloaded 21 Apr 2006 to 132.70.50.117. Redistribution subject to AIP license or copyright, see http://jap.aip.org/jap/copyright.jsp

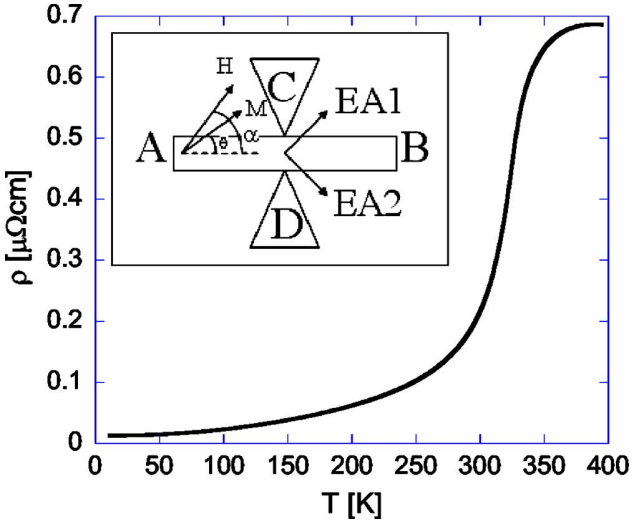

FIG. 1. Resistivity vs temperature of an epitaxial LSMO sample. The peak temperature is at ~390 K. Inset: The pattern used for the experiments. The two easy axes are EA1 and EA2. The angle between the applied magnetic field **H** and the current path is denoted α, and the angle between the magnetization **M** and the current path is denoted θ.

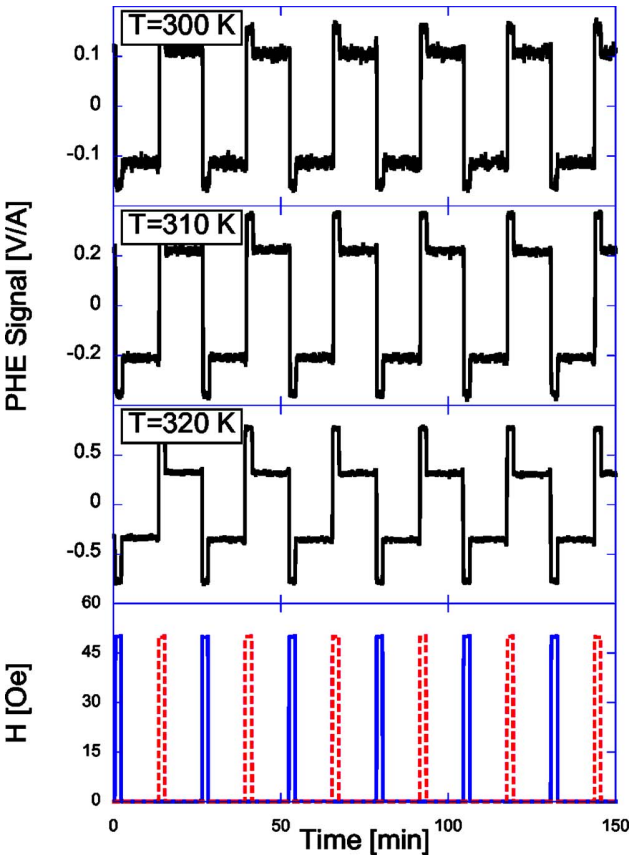

FIG. 2. Planar Hall signal in a LSMO film vs time at different temperatures. A 50 Oe magnetic field is applied parallel to one of the easy axes (EA2). The field aligns the magnetization along this axis, and a negative signal is observed. The magnetic field is then turned off, leaving the magnetization in its remanent state along this axis. After 10 min, the magnetic field is pulsed on and then off, this time parallel to the other easy axis, which leaves the magnetization in remanent state along EA1. This leads to a positive signal reading. This procedure is repeated several times. The bottom graph shows the magnitudes of the magnetic field directed along EA1 (dashed line) and the magnitudes of the magnetic field directed along EA2 (solid line).

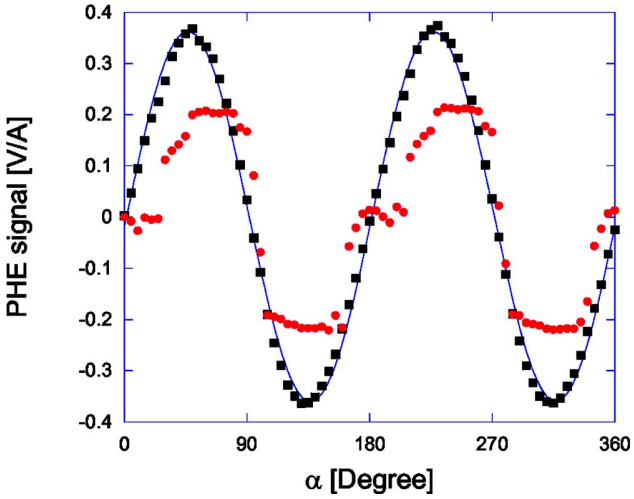

FIG. 3. Planar Hall signal as a function of α with (squares) and without (circles) an applied 50 Oe magnetic field directed at α with respect to the current path. The line connecting the squares is a fit to Eq. (2).

temperatures of 300, 310, and 320 K. The temperature dependence of the transverse voltage shows that the signal increases with temperature up to $T=320$ K. In the low-temperature regime, the effect is measurable down to $T=270$ K. We see that the two memory states are clearly separated and stable in time.

We notice that the PHE signal decreases in absolute value when the field is removed. To explore the origin of this behavior we measured R_{CD} with and without magnetic field as a function of α, the angle between the magnetic field and the current (Fig. 3). The applied field (50 Oe) is bigger than the coercive field of the sample. Therefore, when the field is on, the magnetization is parallel to the applied field and R_{CD} follows the behavior expected from Eq. (2). In the absence of the magnetic field, we see that R_{CD} has several plateaus, which we attribute to biaxial magnetocrystalline anisotropy with easy axes along $\theta \sim 75°$ and $\theta \sim 105°$, combined with shape anisotropy along the current path. The role of shape anisotropy was revealed by measuring patterns with current paths in different orientations. While the effect of these anisotropies decreases the observed signal, the results presented in Fig. 2 indicate that the two magnetic states are still well separated.

The results presented here demonstrate the potential of using the PHE as the basis for a new type of MRAM. The device possesses structural simplicity (a single-layer thin film compared to a tunnel junction), and the measured voltages involve a sign reversal between the two states.

One of the authors (L.K.) acknowledges support by Intel-Israel and by the Israel Science Foundation founded by the Israel Academy of Sciences and Humanities. He and another author (C.A.) acknowledge support from the United States - Israel Binational Science Foundation (BSF), Jerusalem, Israel (Grant No. 2002384).

[1]J. S. Moodera, L. R. Kinder, T. M. Wong, and R. Meservey, Phys. Rev. Lett. **74**, 3273 (1995).
[2]T. Miyazaki and N. Tezuka, J. Magn. Magn. Mater. **151**, 403 (1995).
[3]S. S. P. Parkin, C. Kaiser, A. Panchula, P. M. Rice, B. Hughes, M. Samant,

Downloaded 21 Apr 2006 to 132.70.50.117. Redistribution subject to AIP license or copyright, see http://jap.aip.org/jap/copyright.jsp

and S.-H. Yang, Nat. Mater. **3**, 862 (2004).
[4]S. Yuasa, T. Nagahama, A. Fukushima, Y. Suzuki, and K. Ando, Nat. Mater. **3**, 868 (2004).
[5]C. Goldberg and R. E. Davis, Phys. Rev. **94**, 1121 (1954); F. G. West, J. Appl. Phys. **34**, 1171 (1963); W. M. Bullis, Phys. Rev. **109**, 292 (1958).
[6]T. R. McGuire and R. I. Potter, IEEE Trans. Magn. **11**, 1018 (1975).
[7]B. Zhao, X. Yan, and A. B. Pakhomov, J. Appl. Phys. **81**, 5527 (1997); A. Nemoto, Y. Otani, S. G. Kim, K. Fukamichi, O. Kitakami, and Y. Shimada Appl. Phys. Lett. **74**, 4026 (1999); G. Li, T. Yang, Q. Hu, H. Jiang, and W. Lai, Phys. Rev. B **65**, 134421 (2002); Z. Q. Lu and G. Pan, Appl. Phys. Lett. **80**, 3156 (2002); S. Das, H. Yoshikawa, and S. Nakagawa, J. Appl. Phys. **93**, 8098 (2003).
[8]A. Schuhl, F. Nguyen Van Dau, and J. R. Childress, Appl. Phys. Lett. **66**, 2751 (1995).
[9]H. X. Tang, R. K. Kawakami, D. D. Awschalom, and M. L. Roukes, Phys. Rev. Lett. **90**, 107201 (2003).
[10]Y. Bason, L. Klein, J.-B. Yau, X. Hong, and C. H. Ahn, Appl. Phys. Lett. **84**, 2593 (2004).

Downloaded 21 Apr 2006 to 132.70.50.117. Redistribution subject to AIP license or copyright, see http://jap.aip.org/jap/copyright.jsp

5.4 Planar Hall effect in epitaxial thin films of magnetite

Planar Hall effect in epitaxial thin films of magnetite

Y. Bason[a)] and L. Klein
Department of Physics, Bar Ilan University, Ramat Gan 52900, Israel

H. Q. Wang, J. Hoffman, X. Hong, V. E. Henrich, and C. H. Ahn
Department of Applied Physics, Yale University, New Haven, Connecticut 06520-8284

(Presented on 9 January 2007; received 31 October 2006; accepted 18 December 2006; published online 4 May 2007)

We measured the planar Hall effect (PHE) of magnetite (Fe_3O_4) films between 150 and 350 K. The PHE was measured both with a constant magnetic field rotating in the plane of the sample and in a remanent state after applying a field in specific directions. The PHE amplitude decreases with temperature; however, it changes little between 300 and 350 K. The remanent PHE signal is as high as 10 V/A, larger than previously observed in manganite films. We also measured the PHE in the remanent state and found that its magnitude and stability make it a viable candidate for magnetic random access memory applications. © *2007 American Institute of Physics*.
[DOI: 10.1063/1.2712053]

Magnetite (Fe_3O_4) has been a highly studied oxide in recent years because of its intriguing transport properties.[1] This compound is believed to be half metallic, namely, fully spin polarized at the Fermi level. Consequently, there have been hopes that magnetic tunnel junctions with magnetite films would exhibit exceptionally high magnetoresistance signals, which are useful for spintronic applications such as magnetic random access memory (MRAM). However, magnetic tunnel junctions fabricated with Fe_3O_4 electrodes show only small magnetoresistances, possibly due to spin flips at the interface with the insulating layer or because of the presence of a reduced oxide at this interface.[2] In this work, we explore a potential use for magnetite films for MRAM based on the planar Hall effect (PHE).[3]

The PHE in magnetic conductors occurs when the resistivity depends on the angle θ between the current density **J** and the magnetization **M**, an effect known as anisotropic magnetoresistance (AMR).[4] The AMR yields a transverse electric field when **J** is not parallel or perpendicular to **M**. If we assume **J** is in the x direction and **M** is in the x-y plane, the generated electric field has both a longitudinal component,

$$E_{xx} = \rho_\perp j_x + (\rho_\parallel - \rho_\perp) j_x \cos^2 \theta, \tag{1}$$

and a transverse component,

$$E_y = (\rho_\parallel - \rho_\perp) j_x \sin \theta \cos \theta, \tag{2}$$

where $\rho_\parallel$ and $\rho_\perp$ are the resistivities for magnetization parallel and perpendicular to the current, respectively. The latter component is called the planar Hall effect. Unlike the ordinary and extraordinary Hall effects, the PHE shows an even response upon inversion of **J** and **M**. Therefore, the PHE is most noticeable when **M** changes its axis of orientation, in particular, between $\theta=45°$ and $\theta=-45°$.

The PHE was reported for 3d ferromagnetic metals such as Fe, Co, and Ni.[8] It was used as a tool for studying the in-plane magnetization of samples[5,6] and for applications as low magnetic field sensors.[7] Large PHE signals that are four orders of magnitude larger than in ferromagnetic metals were observed recently, first at low temperatures in the magnetic semiconductor (Ga, Mn)As,[9] then at higher temperatures and even at room temperature in thin films of manganites ($La_{1-x}Sr_xMnO_3$) (Ref. 10) and magnetite.[11] The large PHE effect seen in these materials has been denoted the giant planar Hall effect (GPHE).

In this work we show the GPHE in magnetite films at temperatures ranging from 150 to 350 K, and we demonstrate the potential use of magnetite films for nonvolatile magnetic memory applications based on this effect.

The sample we studied is a 9 nm thick magnetite film deposited by molecular beam epitaxy on a single-crystal MgO (100) substrate. Fe was evaporated from a high temperature effusion cell with an alumina crucible containing 99.995% pure Fe slugs. At the substrate temperature of 523 K, Fe was deposited with a rate of ~0.6 Å/s and in oxygen excited by an electron cyclotron resonance (ECR) plasma source using an O_2 partial pressure of $2x10^{-6}$ Torr. The quality of the sample was determined using surface characterization techniques [reflection high energy electron diffraction (RHEED), low energy electron diffraction (LEED), and x-ray photoelectron spectroscopy (XPS)] and resistivity measurements, which exhibit a change in resistivity at the Verwey transition (T_v=122 K) of close to two orders of magnitude. The film was patterned into a Hall bar shape (see inset of Fig. 1), and the active area (between C and D) on the current path is $10\times 10\ \mu m^2$.

Figure 1 shows the transverse resistivity ρ_{xy} of the magnetite film with a constant magnetic field applied and rotated in the plane of the film. ρ_{xy} is presented as a function of θ, the angle between the magnetization and the current path. The magnetic field is larger than the coercive field of the sample magnetization; hence M is parallel to the field. The measurements were repeated at several temperatures.

[a)]Electronic mail: basony@mail.biu.ac.il

 © 2007 American Institute of Physics

Downloaded 29 Jan 2009 to 132.70.50.117. Redistribution subject to AIP license or copyright; see http://jap.aip.org/jap/copyright.jsp

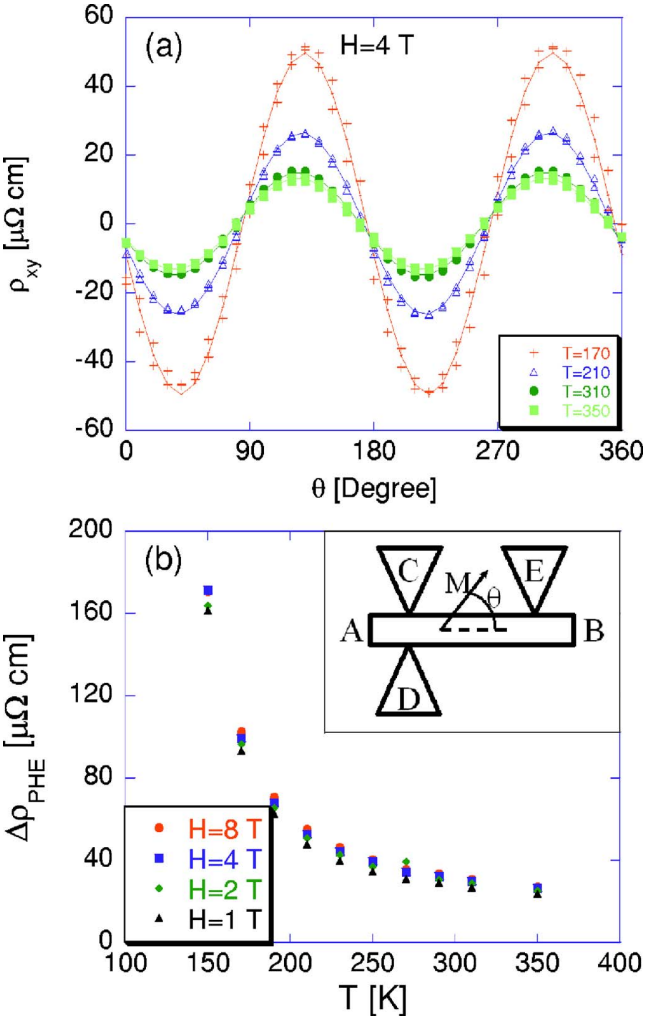

FIG. 1. (Color online) PHE measurements of a magnetite film. (a) Transverse resistivity ρ_{xy} vs θ, the angle between the current and the magnetization, at different temperatures with an applied field of 4 T. The curve is a fit to Eq. (2). (b) $\Delta\rho_{\mathrm{PHE}}$, the amplitude of the PHE signal, at different temperatures and magnetic fields. Inset: A sketch of the pattern used for measurements.

Because of slight misalignment of the transverse leads, a longitudinal component is subtracted from the transverse signal measured between C and D. We can see that the PHE data fit Eq. (2) for the entire temperature range. We note that the amplitude of the PHE signal decreases as the temperature increases. However, in the temperature interval important for applications, 300–340 K, the signal decreases by only ~10%.

For MRAM applications it is important to explore the PHE signal in the remanent state. We magnetize the film in directions that yield maximum PHE signals, ($\theta=\pm 45°$) and measure the signal after the field is removed. Figure 2 shows the PHE signals with and without the external magnetic field. The results are shown for several temperatures. Removing the magnetic field lowers the PHE signal. However, the signal is still quite large, 9 V/A at 300 K, and it remains stable over 30 min of our measurement.

The results presented here show the potential use of magnetite thin films as the basis for a magnetic memory bit,

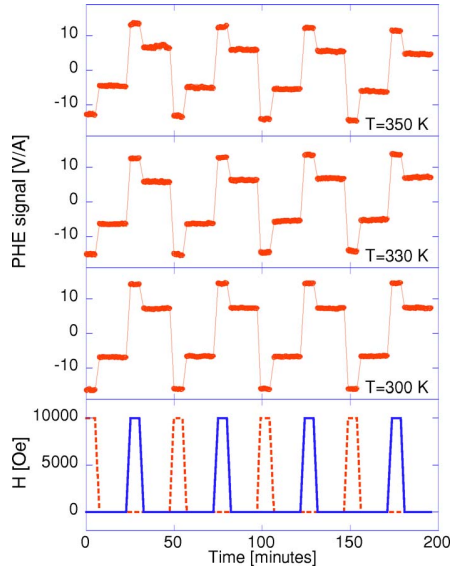

FIG. 2. (Color online) PHE signal measured for 200 min at several temperatures with a changing magnetic field. A field of 1 T is first pulsed at $\theta=-45°$ and aligns the sample magnetization in this direction. A negative PHE signal is observed. The magnetic field is then removed, leaving the magnetization in its remanent state. After 30 min, the field is pulsed again, this time at $\theta=45°$, and a positive PHE signal is observed. The process is repeated several times. The lower graph shows the amplitude of the magnetic field along $\theta=45°$ (solid line) and $\theta=-45°$ (dashed line).

where the two magnetization orientations at $\theta=\pm 45°$ correspond to the two memory states. The different PHE signals are clearly distinguishable at temperatures as high as 350 K and remain stable over time.

One of the authors (L.K.) acknowledges support by the Israel Science Foundation founded by the Israel Academy of Sciences and Humanities. Another author (C. A.) acknowledges primary support from the National Science Foundation under Contract Nos. MRSEC DMR 0520495 and DMR 0134721 and ONR, along with support from the Packard and Sloan Foundations. Another one of the author (V.E.H.) acknowledges support from the National Science Foundation under Contract No. MRSEC DMR 0520495 and the U.S. Department of Energy Grant No. DE-FG02-OOER45844.

[1]M. Ziese, Phys. Rev. B **62**, 1044 (2000); B. A. Calhoun, Phys. Rev. **94**, 1577 (1954); A. Kozl/owski, R. J. Rasmussen, J. E. Sabol, P. Metcalf, and J. M. Honig, Phys. Rev. B **48**, 2057 (1993).
[2]X. W. Li, G. Xiao, W. Qiam, and V. P. Dravid, Appl. Phys. Lett. **73**, 3282 (1998).
[3]Y. Bason, L. Klein, J.-B. Yau, X. Hong, J. Hoffman, and C. H. Ahn, J. Appl. Phys. **99**, 08R701 (2006).
[4]T. R. McGuire and R. I. Potter, IEEE Trans. Magn. **11**, 1018 (1975).
[5]G. Li, T. Yang, Q. Hu, H. Jiang, and W. Lai, Phys. Rev. B **65**, 134421 (2002).
[6]S. Das, H. Yoshikawa, and S. Nakagawa, J. Appl. Phys. **93**, 8098 (2003).
[7]A. Schul, F. Nguyen Van Dau, and J. R. Childress, Appl. Phys. Lett. **66**, 2751 (1995).
[8]C. Goldberg and R. E. Davis, Phys. Rev. **94**, 1121 (1954); F. G. West, J. Appl. Phys. **34**, 1171 (1963); W. M. Bullis, Phys. Rev. **109**, 292 (1958).
[9]H. X. Tang, R. K. Kawakami, D. D. Awschalom, and M. L. Roukes, Phys. Rev. Lett. **90**, 107201 (2003).
[10]Y. Bason, L. Klein, J.-B. Yau, X. Hong, and C. H. Ahn, Appl. Phys. Lett. **84**, 2593 (2004).
[11]X. Jin, R. Ramos, Y. Zhou, C. McEvoy, and I. V. Shvets, J. Appl. Phys. **99**, 08C509 (2006).

Downloaded 29 Jan 2009 to 132.70.50.117. Redistribution subject to AIP license or copyright; see http://jap.aip.org/jap/copyright.jsp

5.5 The magnetoresistance tensor of $La_{0.8}Sr_{0.2}MnO_3$

The magnetoresistance tensor of $La_{0.8}Sr_{0.2}MnO_3$

Y. Bason[1],* J. Hoffman[2], C. H. Ahn[2], and L. Klein[1]
[1]*Department of Physics, Nano-magnetism Research Center, Institute of Nanotechnology and Advanced Materials, Bar-Ilan University, Ramat-Gan 52900, Israel and*
[2]*Department of Applied Physics, Yale University, New Haven, Connecticut 06520-8284, USA*
(Dated: December 21, 2008)

We measure the temperature dependence of the anisotropic magnetoresistance (AMR) and the planar Hall effect (PHE) in c-axis oriented epitaxial thin films of $La_{0.8}Sr_{0.2}MnO_3$, for different current directions relative to the crystal axes, and show that both AMR and PHE depend strongly on current orientation. We determine a magnetoresistance tensor, extracted to 4th order, which reflects the crystal symmetry and provides a comprehensive description of the data. We extend the applicability of the extracted tensor by determining the bi-axial magnetocrystalline anisotropy in our samples.

PACS numbers: 75.47.-m, 75.47.Lx, 72.15.Gd, 75.70.Ak

I. INTRODUCTION

The interplay between spin polarized current and magnetic moments gives rise to intriguing phenomena that have led to the emergence of the field of spintronics [1]. In most cases, the materials used to study these phenomena have been amorphous alloys of 3d itinerant ferromagnets (e.g., permalloy), while much less is known about the behavior in more complicated crystalline systems. Manganites, which are magnetic perovskites, serve as a good example for such a system. As we will show, elucidating these phenomena in this material system provides tools for better theoretical understanding of spintronics phenomena and reveals opportunities for novel device applications.

The magnetotransport properties of manganites, which are known for their colossal magnetoresistance [2] have been extensively studied; nevertheless, despite numerous studies devoted to elucidating the role of the magnitude of the magnetization, relatively few reports have addressed the role of the *orientation* of the magnetization, which is known to affect both the longitudinal resistivity ρ_{long} (anisotropic magnetoresistance effect - AMR) and transverse resistivity ρ_{trans} (planar Hall effect - PHE).

For conductors that are amorphous magnetic films, the dependence of ρ_{long} and ρ_{trans} on the magnetic orientation is given by:

$$\rho_{long} = \rho_\perp + (\rho_\parallel - \rho_\perp)\cos^2\varphi \tag{1}$$

and

$$\rho_{trans} = (\rho_\parallel - \rho_\perp)\sin\varphi\cos\varphi \tag{2}$$

where φ is the angle between the current $\mathbf{J}$ and the magnetization $\mathbf{M}$ and $\rho_\parallel$ and $\rho_\perp$ are the resistivities parallel and perpendicular to $\mathbf{M}$, respectively [3–6]. Eqs. 1 and 2 are not expected to apply to crystalline conductors, as they are independent of the crystal axes [7]. Nevertheless, they have been used to describe AMR and PHE in epitaxial films [8–11]; qualitative and quantitative deviations were occasionally attributed to extrinsic effects.

Here, we quantitatively identify the crystalline contributions to AMR and PHE in epitaxial films of $La_{0.8}Sr_{0.2}MnO_3$ (LSMO) and replace Eqs. 1 and 2 with equations that provide a comprehensive description of the magnetotransport properties of LSMO. The equations are derived by expanding the resistivity tensor to 4th order and keeping terms consistent with the crystal symmetry.

AMR and PHE in manganites constitute an important aspect of their magnetotransport properties; hence, quantitative determination of these effects is essential for comprehensive understanding of the interplay between magnetism and transport in this class of materials. In addition, when the dependence of AMR and PHE on local magnetic configurations is known, the two effects can be used as a powerful tool for probing and tracking static and dynamic magnetic configurations in patterned structures. Moreover, as the magnitude of the AMR and PHE changes dramatically with current direction, the elucidation of the appropriate equations is crucial for designing novel devices with optimal properties that are based on these phenomena.

II. EXPERIMENT

We present here results measured on epitaxial thin films (~ 40 nm) of $La_{0.8}Sr_{0.2}MnO_3$ with a Curie temperature (T_c) of ~ 290 K grown on cubic single crystal [001] $SrTiO_3$ substrates using off-axis magnetron sputtering. $\theta - 2\theta$ x-ray diffraction reveals c-axis oriented growth (in the pseudocubic frame), with an out-of-plane lattice constant of ~ 0.3876 nm, and an in-plane lattice constant of ~ 0.3903 nm, consistent with coherently strained films. No impurity phases are detected. Rock-

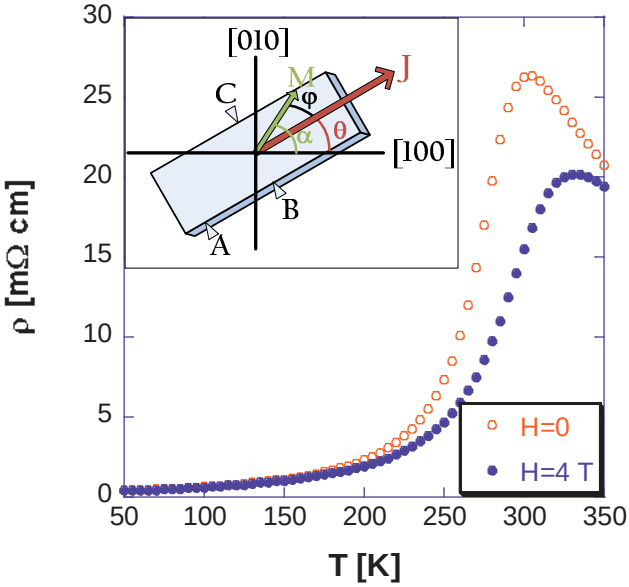

FIG. 1: ρ vs. T with (solid circles) and without (empty circles) an applied magnetic field of H=4 T. Inset: Sketch of the relative orientations of the current density **J**, magnetization **M**, and the crystallographic axes. ρ_{long} is measured between A and B, ρ_{trans} is measured between B and C.

ing curves taken around the 001 and 002 reflections have a typical full width at half maximum of 0.05°. The film surfaces have been characterized using atomic force microscopy, which shows a typical root-mean-square surface roughness of ~ 0.2 nm. The samples were patterned using photolithography to create 7 patterns on the same substrate. Each pattern has its current path at a different angle θ relative to the [100] direction ($\theta = 0°, 15°, 30°, 45°, 60°, 75°, 90°$), with electrical leads that allow for AMR and PHE measurements (see figure 1). ρ_{long} and ρ_{trans} data obtained by applying a magnetic field of H=4 T in the plane of the film and rotating the sample around the [001] axis.

III. RESULTS AND DISCUSSION

Fig. 2 presents ρ_{long} and ρ_{trans} for all seven patterns at T=5, 125 and 300 K. At T = 300 K both ρ_{long} and ρ_{trans} seem to behave according to Eqs. 1 and 2. However, contrary to these equations, the amplitude of ρ_{long} differs from the amplitude of ρ_{trans}; moreover, they both change with θ, the angle between **J** and [100].

The discrepancies increase as the temperature decreases, and at T=125 K the variations in the amplitudes for measurements taken for different θ increase. Furthermore, the location of the extremal points are dominated by α, the angle between **M** and [100]. At T = 5 K, the deviations are even more evident as the AMR measurements are no longer described with a sinusoidal curve. All these observations clearly indicate the need for a higher order tensor to adequately describe the magnetotransport behavior of LSMO.

The resistivity tensor in a magnetic conductor depends on the direction cosines, α_i, of the magnetization vector, and can be expressed as a series expansion of powers of the α_i [12], giving:

$$\rho_{ij}(\alpha) = \sum_{k,l,m...=1}^{3} (a_{ij} + a_{kij}\alpha_k + a_{klij}\alpha_k\alpha_l + \\ + a_{klmij}\alpha_k\alpha_l\alpha_m + a_{klmnij}\alpha_k\alpha_l\alpha_m\alpha_n + ...) \quad (3)$$

where $i, j = 1, 2, 3$ and the a's are expansion coefficients. As usual $\rho_{ij}(\alpha) = \rho^s_{ij}(\alpha) + \rho^a_{ij}(\alpha)$ where ρ^s_{ij} and ρ^a_{ij} are symmetric and antisymmetric tensors, respectively. As both AMR and PHE are symmetric, we use only ρ^s_{ij} for their expression. As we are interested only in the in-plane properties, we use the tensor expansion for crystals with m3m cubic-crystal structure [13]. The 4th order symmetric resistivity tensor ρ^s for this class of materials in the xy plane (as **M**, **J** and the measurements are all in the plane of the film) is given by:

$$\rho^s = \begin{pmatrix} C' + C'_1\alpha_1^2 + C'_2\alpha_1^4 & C'_4\alpha_1\alpha_2 \\ C'_4\alpha_1\alpha_2 & C' + C'_1\alpha_2^2 + C'_2\alpha_2^4 \end{pmatrix}. \quad (4)$$

When **J** is along θ we obtain:

$$\rho_{long} = A\cos(2\alpha - 2\theta) + B\cos(2\alpha + 2\theta) + C\cos(4\alpha) + D \quad (5)$$

and

$$\rho_{trans} = A\sin(2\alpha - 2\theta) - B\sin(2\alpha + 2\theta) \quad (6)$$

with:
$A = (C'_1 + C'_2 + C'_4)/4$
$B = (C'_1 + C'_2 - C'_4)/4$
$C = C'_2/8$
$D = C' + C'_1/2 + 3C'_2/8$

Equations 5 and 6, which take into account the crystal symmetry, have 4 independent parameters (A, B, C and D) with which we fit (as shown in Figure 2) at any given temperature and magnetic field a set of 14 different curves (7 AMR curves and 7 PHE curves).

The parameter A is a coefficient of a term describing a non-crystalline contribution since $(\alpha - \theta)$ is the angle between **M** and **J** irrespective of their orientation relative to the crystal axes. On the other hand, the parameters B and C are coefficients of terms that depend on the orientation of **M** and/or **J** relative to the crystal axes.

We note that adding the terms with the coefficient B (in both Eq. 5 and 6) to the "A" term changes only the amplitude and the phase of the signal compared to Eqs. 1 and 2: Eq. 5 can be written (for C=0) as:

$$\rho_{long} = E\cos(2\alpha - \phi_{long}) + D \quad (7)$$

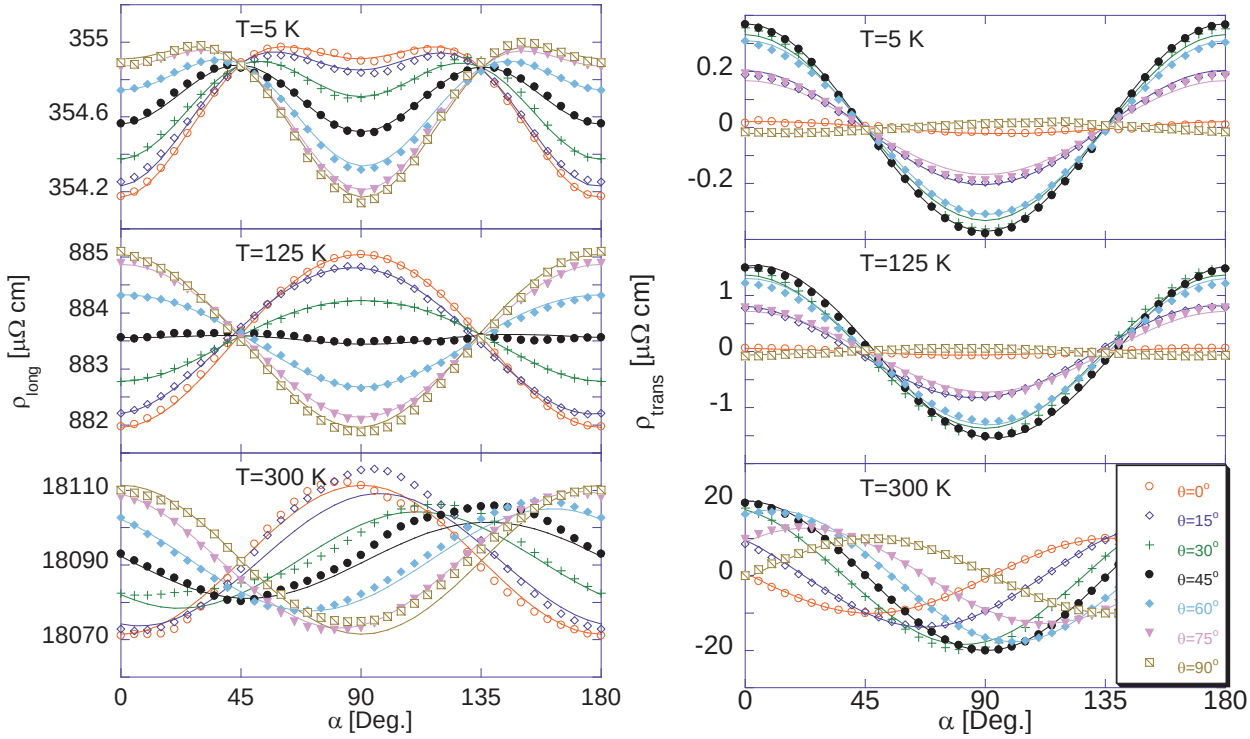

FIG. 2: Longitudinal resistivity ρ_{long} (left) and transverse resistivity ρ_{trans} (right) vs. α, the angle between the magnetization and [100], for different angles θ (the angle between the current direction and [100]) at different temperatures with an applied magnetic field of 4 T. The solid lines are fits to Eqs. 5 and 6.

where $E^2 = A^2 + B^2 + 2AB\cos 4\theta$ and $\sin\phi_{long} = \frac{A-B}{E}\sin(2\theta)$; and Eq. 6 can be written as:

$$\rho_{trans} = F\sin(2\alpha - \phi_{trans}) \tag{8}$$

where $F^2 = A^2 + B^2 - 2AB\cos 4\theta$ and $\sin\phi_{trans} = \frac{A+B}{F}\sin 2\theta$. The amplitude of $\rho_{trans}(\alpha)$, F, varies with θ between a maximal value of $|A+B|$ for $\theta = \pm 45°$ and a minimal value of $|A-B|$ for $\theta = 0, \pm 90°$. On the other hand, the amplitude of $\rho_{long}(\alpha)$, E, obtains its maximal value $|A+B|$ at $\theta = 0, \pm 90°$ and its minimal value $|A-B|$ at $\theta = \pm 45°$. When the C term is added it does not affect ρ_{trans}; however, ρ_{long} behaves qualitatively differently.

We thus observe that the current direction affects quite dramatically the amplitude of the effect. At 125 K, for instance, the PHE amplitude for current at 45° relative to [100] is more than 20 times larger than the PHE for current parallel to [100]. This means that appropriate selection of the current direction that takes into consideration crystalline effects is important for designing devices that use the PHE for magnetic sensor or magnetic memory applications [14].

Figure 3 presents the temperature dependence of B/A and C/A. Close to T_c both B and C are negligible relative to A; therefore, AMR and PHE measurements appear to fit Eqs. 1 and 2. At intermediate temperatures where C is still much smaller than A (while B and A are of the same order), the signal remains sinusoidal, although its deviation from Eqs. 1 and 2 becomes quite evident. At low temperatures, C is on the order of B, and the AMR signal is no longer sinusoidal.

We have performed similar measurements using LSMO films with various doping levels as well as films of $La_{1-x}Ca_xMnO_3$. The results clearly indicate the failure of Eqs. 1 and 2 and the applicability of Eqs. 5 and 6. These results will be addressed elsewhere. We also note that when **J** is along one of the crystal axes (i.e., $\theta = 0, 90°$) equation 5 reduces to $\rho_{long} = a_0 + a_1\cos^2\alpha + a_2\cos^4\alpha$, a form used before to describe the crystal contributions in various magnetic films including epitaxial films of Fe [15] and Fe_3O_4 [16]. Therefore, it appears that Eqs. 5 and 6 may be applicable to a wide range of materials.

Going back to $La_{0.8}Sr_{0.2}MnO_3$, we would like to address the case when the AMR and PHE measurements are performed with low applied magnetic fields, where **M** is no longer parallel to **H**, due to intrinsic magnetocrystalline anisotropy.

Our LSMO films exhibit bi-axial magnetocrystalline anisotropy with easy axes along ⟨110⟩ directions, a manifestation of in-plane cubic symmetry. When a field **H** is applied, the total free energy consists of the magnetocrystalline anisotropy energy and the Zeeman energy:

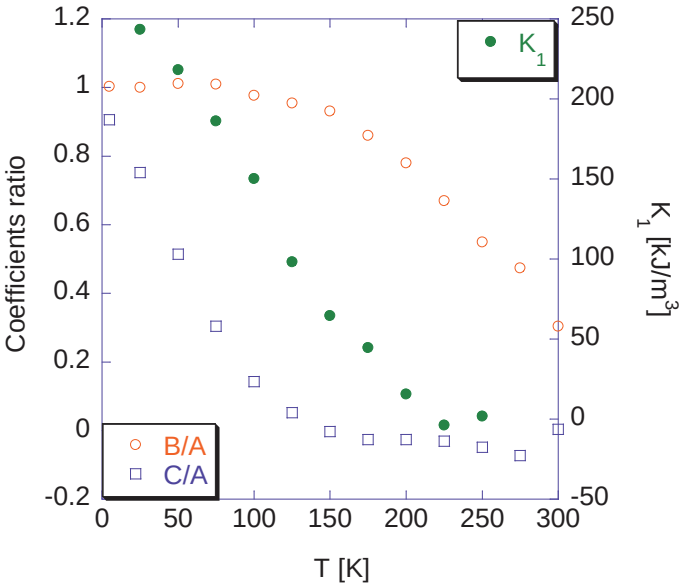

FIG. 3: The ratios of the coefficients from Eqs. 5 and 6 (B/A and C/A) (left axis) and the coefficient K_1 from Eq. 9 (right axis) as a function of temperature.

$$E = \frac{K_1}{4}\cos^2 2\alpha - MH\cos(\alpha - \beta) \qquad (9)$$

where K_1 is the magnetocrystalline anisotropy energy and β is the angle between **H** and [100]. The first term is responsible for the bi-axial magnetocrystalline anisotropy with easy axes along $\alpha = \pm 45°$ and $\alpha = \pm 135°$. We have determined the value of K_1 at various temperatures (see Fig. 3) by switching the magnetization between the two easy axes (see Fig. 4). The extracted value of K_1 allows us by using Eqs. 5, 6 and 9 to fit the AMR and PHE data obtained with relatively low applied fields (e.g., 500 Oe), where **M** does not follow **H** (see Fig. 4).

IV. CONCLUSION

In summary, we have expanded the magnetoresistance tensor to 4th order keeping terms consistent with the symmetry of epitaxial films of LSMO and derived equations that provide a comprehensive description of AMR and PHE in LSMO films in a wide range of temperatures. The results shed new light on the interplay between magnetism and electrical transport in this class of materials and may serve as a basis for further study of the microscopic origin of magnetotransport properties of LSMO and other manganites. The results contribute to the ability to monitor magnetic configurations via magnetotransport properties, a feature of particular importance in studying nano-structures, and will facilitate the design of novel devices that use AMR and PHE.

ACKNOWLEDGMENTS

We acknowledge useful discussions with E. Kogan. L.K. acknowledges support by the Israel Science Foundation founded by the Israel Academy of Sciences and Humanities. Work at Yale supported by NSF MRSEC DMR 0520495, DMR 0705799, NRI, ONR, and the Packard Foundation.

* Electronic address: basony@mail.biu.ac.il

[1] G. A. Prinz, Science **282**, 1660 (1998).
[2] M. McCormack, S. Jin, T H. Tiefel, R. M. Fleming, J. M. Phillips and R. Ramesh, Appl. Phys. Lett. **64**, 3045 (1994).
[3] C. Goldberg and R. E. Davis, Phys. Rev. **94**, 1121 (1954).
[4] F. G. West, J. Appl. Phys. **34**, 1171 (1963).
[5] W. M. Bullis, Phys. Rev. **109**, 292 (1958).
[6] T. R. McGuire and R. I. Potter, IEEE Trans. Magn. **11**, 1018 (1975).
[7] Döring, W., Ann. Physik **(**32) (1938) 259.
[8] X. Jin, R. Ramos, Y. Zhou, C. McEvoy, and I. V. Shvets, J. Appl. Phys. **99**, 08C509 (2006).
[9] H. X. Tang, R. K. Kawakami, D. D. Awschalom, and M. L. Roukes, PRL **90**,107201 (2003).
[10] Y. Bason, L. Klein, J.-B. Yau, X. Hong, and C. H. Ahn, Appl. Phys. Lett. **84**, 2593 (2004).
[11] I.C. Infante, V. Laukhin, F. Sánchez, J. Fontcuberta, Materials Science and Engineering B **126** (2006) 283-286.
[12] T. T. Chen, V. A. Marsocii, Physica **59** (1972) 498-509.
[13] Birss, R. R., Symmetry and Magnetizm, North-Holland Publ. Comp. (Amsterdam, 1964).
[14] Y. Bason, L. Klein, J.-B. Yau, X. Hong, J. Hoffman, and C. H. Ahn, J. Appl. Phys. **99**, 08R701 (2006).
[15] R. P. van Gorkom, J. Caro, T. M. Klapwijk, and S. Radelaar, Physical Review B **63**, 134432 (2001).
[16] R. Ramos, S. K. Arora, and I. V. Shvets, PRB **78**, 214402 (2008).

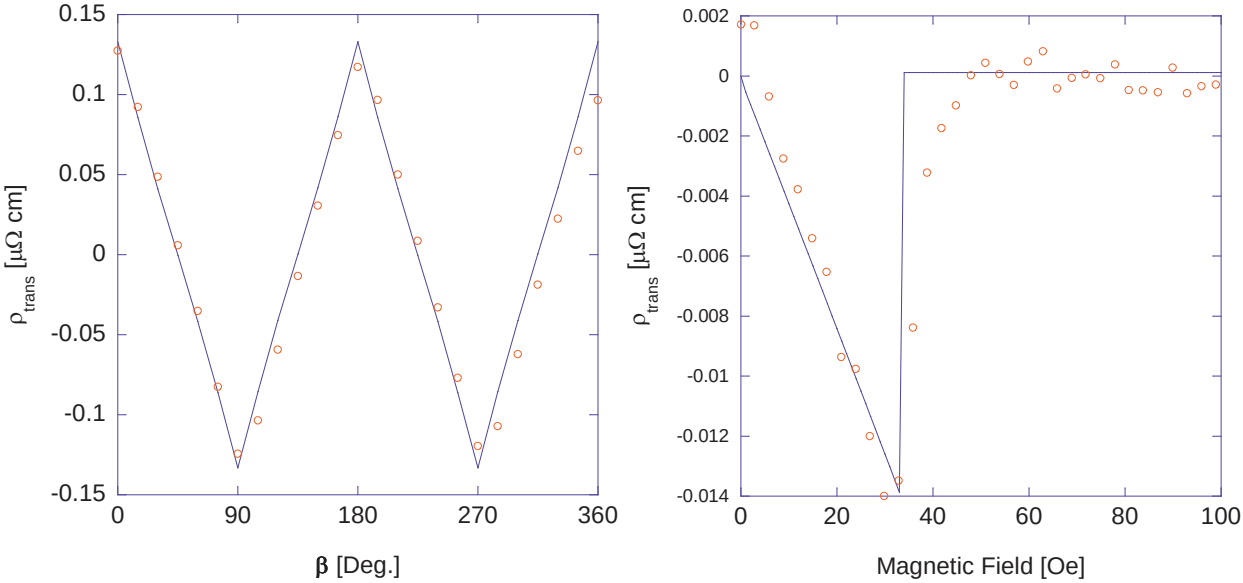

FIG. 4: Left: PHE signal as a function of β, the magnetic field direction relative to the [100] (H=500 Oe and T=50 K). The line is a fit to Eq. 6 with α extracted using Eq. 9. Right: PHE as a function of magnetic field. The sample is prepared with **M** along [100], and the field is applied along $[1\bar{1}0]$. The line is a fit using Eq. 9.

Bibliography

[1] N. F. Mott, Proceedings of the Royal Society of London. Series A, Mathematical and Physical Sciences (1934-1990) **153**, 699 (1936).

[2] C. Goldberg and R. E. Davis, Phys. Rev. **94**, 1121 (1954).

[3] T. McGuire and R. Potter, Magnetics, IEEE Transactions on **11**, 1018 (1975).

[4] B. Zhao, X. Yan, and A. B. Pakhomov, J. Appl. Phys. **81**, 5527 (1997).

[5] A. Nemoto *et al.*, Applied Physics Letters **74**, 4026 (1999).

[6] G. Li, T. Yang, Q. Hu, H. Jiang, and W. Lai, Phys. Rev. B **65**, 134421 (2002).

[7] Z. Q. Lu and G. Pan, Applied Physics Letters **80**, 3156 (2002).

[8] S. Das, H. Yoshikawa, and S. Nakagawa, J. Appl. Phys. **93**, 8098 (2003).

[9] A. Schuhl, F. N. V. Dau, and J. R. Childress, Applied Physics Letters **66**, 2751 (1995).

[10] H. X. Tang, R. K. Kawakami, D. D. Awschalom, and M. L. Roukes, Physical Review Letters **90**, 107201 (2003).

[11] S. D. Sarma, Nature Materials **2**, 292 (2003).

[12] Y. Bason, L. Klein, J.-B. Yau, X. Hong, and C. H. Ahn, Applied Physics Letters **84**, 2593 (2004).

[13] C. Vouille *et al.*, Phys. Rev. B **60**, 6710 (1999).

[14] J. S. Moodera, L. R. Kinder, T. M. Wong, and R. Meservey, Physical Review Letters **74**, 3273 (1995).

[15] S. A. Wolf *et al.*, Science **294**, 1488 (2001).

[16] W. Döring, Annalen der Physik **424**, 259 (1938).

[17] X. Jin, R. Ramos, Y. Zhou, C. McEvoy, and I. V. Shvets, Applied Physics Letters **99**, 08C509 (2006).

[18] K.-J. Friedland, J. Herfort, P. K. Muduli, H.-P. Schnherr, and K. H. Ploog, Journal of Superconductivity and Novel Magnetism **18**, 309 (2005).

[19] I. Infante, V. Laukhin, F. Sánchez, and J. Fontcuberta, Materials Science and Engineering: B **126**, 283 (2006).

[20] T. T. Chen and V. A. Marsocci, Physica **59**, 498 (1972).

[21] R. R. Birss, *Symmetry and Magnetizm* (North-Holland Publ. Comp., 1964).

[22] Y. Bason, J. Hoffman, C. Ahn, and L. Klein, arXiv:0810.4679v1 [cond-mat.mtrl-sci].

[23] M. N. Baibich *et al.*, Physical Review Letters **61**, 2472 (1988).

[24] G. Binasch, P. Grünberg, F. Saurenbach, and W. Zinn, Phys. Rev. B **39**, 4828 (1989).

[25] S. S. P. Parkin, Z. G. Li, and D. J. Smith, Applied Physics Letters **58**, 2710 (1991).

[26] T. Miyazaki and N. Tezuka, Journal of Magnetism and Magnetic Materials **151**, 403 (1995).

[27] S. S. P. Parkin *et al.*, Nat. Mater. **3**, 862 (2004).

[28] S. Yuasa, T. Nagahama, A. Fukushima, Y. Suzuki, and K. Ando, Nat. Mater. **3**, 868 (2004).

[29] L. J. Schwee, P. E. Hunter, K. A. Restorff, and M. T. Shephard, Journal of Applied Physics **53**, 2762 (1982).

[30] A. Pohm, J. Daughton, C. Comstock, H. Yoo, and J. Hur, Magnetics, IEEE Transactions on **23**, 2575 (1987).

[31] A. Pohm, J. Huang, J. Daughton, D. Krahn, and V. Mehra, Magnetics, IEEE Transactions on **24**, 3117 (1988).

[32] J. Daughton, Thin Solid Films **216**, 162 (1992).

[33] E. Y. Chen, S. Tehrani, T. Zhu, M. Durlam, and H. Goronkin, Journal of Applied Physics **81**, 3992 (1997).

[34] A. Pohm, B. Everitt, R. Beech, and J. Daughton, Magnetics, IEEE Transactions on **33**, 3280 (1997).

[35] J. M. Daughton, Journal of Applied Physics **81**, 3758 (1997).

[36] S. S. P. Parkin *et al.*, Journal of Applied Physics **85**, 5828 (1999).

[37] P. Naji, M. Durlam, S. Tehrani, J. Calder, and M. DeHerrera, Solid-State Circuits Conference, 2001. Digest of Technical Papers. ISSCC. 2001 IEEE International , 122 (2001).

[38] Y. Bason *et al.*, Journal of Applied Physics **99**, 08R701 (2006).

[39] Y. Bason *et al.*, Journal of Applied Physics **101**, 09J507 (2007).

[40] L. Klein *et al.*, Magnetoelectronic devices based on cmr thin films. U.S. patent (pending).

[41] E. Dagotto, T. Hotta, and A. Moreo, Physics Reports **344**, 1 (2001).

[42] G. H. Jonker and J. H. V. Santen, Physica **16**, 337 (1950).

[43] J. H. V. Santen and G. H. Jonker, Physica **16**, 599 (1950).

[44] R. Kusters, J. Singleton, D. Keen, R. McGreevy, and W. Hayes, Physica B: Condensed Matter **155**, 362 (1989).

[45] R. von Helmolt, J. Wecker, B. Holzapfel, L. Schultz, and K. Samwer, Physical Review Letters **71**, 2331 (1993).

[46] S. Jin *et al.*, Science **264**, 413 (1994).

[47] J. S. Noh *et al.*, Applied Physics Letters **79**, 233 (2001).

[48] C. Zener, Phys. Rev. **81**, 440 (1951).

[49] C. Zener, Phys. Rev. **82**, 403 (1951).

[50] P. W. Anderson and H. Hasegawa, Phys. Rev. **100**, 675 (1955).

[51] P. G. de Gennes, Phys. Rev. **118**, 141 (1960).

[52] L. Neel, Ann. Phys. **3**, 137 (1948).

[53] C. G. Shull, E. O. Wollan, and W. C. Koehler, Phys. Rev. **84**, 912 (1951).

[54] F. Walz, Journal of Physics: Condensed Matter **14**, R285 (2002).

[55] G. K. Rozenberg *et al.*, Physical Review Letters **96**, 045705 (2006).

[56] P. aw Piekarz, K. Parlinski, and A. M. Oleś, Physical Review Letters **97**, 156402 (2006).

[57] J. M. D. Coey, A. E. Berkowitz, L. Balcells, F. F. Putris, and F. T. Parker, Applied Physics Letters **72**, 734 (1998).

[58] M. Ziese, Phys. Rev. B **62**, 1044 (2000).

[59] M. Ziese and H. J. Blythe, Journal of Physics: Condensed Matter **12**, 13 (2000).

[60] D. Reisinger, P. Majewski, M. Opel, L. Alff, and R. Gross, Applied Physics Letters **85**, 4980 (2004).

[61] X. W. Li, A. Gupta, G. Xiao, W. Qian, and V. P. Dravid, Applied Physics Letters **73**, 3282 (1998).

[62] Y. Moritomo, A. Asamitsu, H. Kuwahara, and Y. Tokura, Nature **380**, 141 (1996).

[63] H. W. Zandbergen, S. Freisem, T. Nojima, and J. Aarts, Phys. Rev. B **60**, 10259 (1999).

– PHE שונה ממשרעת ה – AMR (למרות שעל פי המשוואות שתיהן אמורות להיות שוות ל – $(\rho_{\parallel} - \rho_{\perp})$). הערנו, שתרומות הקשורות לגביש יכולות להיות המקור לאי-התאמות אלו. תרומות אלו היו הנושא של עבודתי הבאה, בה פיתחנו משוואות חדשות לתיאור ה – PHE וה – AMR בחומרים גבישיים ע"י פיתוח טנזור ההתנגדות סביב המגנטיזציה ושמירת ערכים המתאימים לסימטריה הגבישית. המשוואות החדשות מצליחות לתאר את כל המדידות שביצענו בשכבות שונות של LSMO. עבודה זו הוגשה לפרסום ב – PRB:

Y. Bason, J. Hoffman, C. H. Ahn, and L. Klein, The magnetoresistance tensor of $La_{0.8}Sr_{0.2}MnO_3$, submitted to PRB.

יישום מעניין נוסף של ה – GPHE הוא זכרון גישה אקראית מגנטי (Magnetic Random Access Memory - MRAM). ל – MRAM תכונות היכולות להפוך אותו לזכרון האידיאלי, מכיוון שבנוסף להיותו לא נדיף (כלומר, הזכרון שומר על ערכו גם בהעדר מתח), הוא אינו מוגבל בכמות הפעמים בהם ניתן לשכתב אותו (בניגוד ל – FLASH), מהיר כמו Static Random Access Memory – SRAM וניתן לצופף אותו כמעט כמו Dynamic Random Access Memory – DRAM. בכדי לשמור סיבית ב – MRAM, צריך לכוון את המגנטיזציה בשכבה מסויימת לאחד משני כיוונים מוגדרים. בכדי לקרוא את הסיבית יש לגלות את כיוון המגנטיזציה. בכדי להשיג מהירות קריאה גבוהה ולשלב תא זיכרון כזה במעגלים אלקטרוניים, יש לוודא שקריאת כיוון המגנטיזציה תתבצע ע"י מדידת התנגדות חשמלית. כיום נהוג לממש תא זיכרון מגנטי בעזרת Magnetic Tunnel Junction – MTJ. ההתנגדות של MTJ יכולה להיות נמוכה או גבוהה, כפונקציה של כיווני המגנטיזציה בשתי שכבות מגנטיות. ב – MTJ מודרני, שינוי ההתנגדות החשמלית בין שני המצבים הוא בערך 200%, אולם המבנה כולל שכבות רבות של חומרים והוא מסובך ויקר לייצור. אנו מציעים שיטה חדשה ליישום תא זיכרון מגנטי המבוססת על ה – GPHE ב – LSMO. תיאור השיטה וניסוי המדגים את יציבות תא בודד בטמפרטורת החדר המיושם בשיטה זו התפרסם ב:

Y. Bason, L. Klein, J.-B. Yau, X. Hong, J. Hoffman ,and C. H. Ahn, Journal of Applied Physics, **99**, 08R701 (2006).

בנוסף ל – LSMO, הדגמנו יישום תא זיכרון מגנטי המבוסס על GPHE גם בחומר גבישי אחר, Fe_3O_4 (Magnetite). בחומר זה ה – GPHE מתקיים בטמפרטורות גבוהות אפילו יותר מאשר ב – LSMO. עבודה זו פורסמה ב:

Y. Bason, L. Klein, H. Q. Wang, J. Hoffman, X. Hong, V. E. Henrich and C. H. Ahn, J. Appl. Phys. **101**, 09J507 (2007).

כזכור, המשואות הפשוטות המתארות את ה – AMR ואת ה – PHE פותחו עבור חומרים אמורפיים, אך נמצאות בשימוש בכדי לתאר את התופעות הללו גם בחומרים גבישיים. כבר בעבודתי הראשונה הצבענו על סטיות מהמשואות הללו. לדוגמה, בניסויים מסויימים, משרעת ה

$E_{trans} = (\rho_{\parallel} - \rho_{\perp}) J \sin\varphi \cos\varphi$. הרכיב הרוחבי, E_{trans} , נקרא אפקט הול המשטחי (planar Hall effect – PHE). משואות פשוטות אלו פותחו עבור חומרים אמורפיים, אך נהוג להשתמש בהם לתיאור AMR ו – PHE גם בחומרים גבישיים, למרות חוסר התאמות מסויימות להן לא יחסו חשיבות.

לאפקט הול המשטחי משרעת קטנה, לכן הוא משך תשומת לב מועטה מאז התגלה. לאחרונה התעוררה מחדש ההתעניינות ב – PHE בעקבות מדידות שבוצעו בחצי מוליך המגנטי GaMn(As). החוקרים מצאו שה – PHE בחומר זה גדול בארבעה סדרי גודל מה – PHE במתכות, ונתנו לו את השם "אפקט הול משטחי ענק" – "Giant planar Hall effect – GPHE". החוקרים גם ציינו את הפוטנציאל היישומי של האפקט, בתנאי שיצליחו להתגבר על מחסום הטמפרטורה – בחצי מוליך המגנטי GaMn(As) התופעה נצפתה רק בטמפרטורות נמוכות מחמישים קלוין.

עבודתי החלה בעקבות תגלית בקבוצת המחקר שלנו, שאפקט הול המשטחי הענק קיים גם במנגניטים. הדגם שאותו מדדנו היה $La_{1-x}Sr_xMnO_3$ (LSMO) ברמת אילוח של x=0.16. אפקט הול המשטחי ב – LSMO גדול כמו זה שנצפה בחצי מוליך המגנטי, אבל מתקיים בטמפרטורות גבוהות בהרבה – עד 140 קלווין. עבודה זו פורסמה ב:

Y. Bason, L.Klein, J. –B. Yau, X. Hong and C. H. Ahn, Appl. Phys. Lett. **84**, 2593 (2004).

מכיון שה – PHE תלוי בזוית שבין המגנטיזציה לשדה המגנטי, ניתן להתייחס אליו כדרך למדידת כיוון המגנטיזציה בדגם ע"י מדידת מתח. ביצענו ניסוי כזה בכדי למצוא את כיווני הצירים הקלים ב – LSMO ברמת אילוח של x=0.16. מצאנו שהצירים הקלים בחומר נמצאים בזויות של $\theta_1 = \pm(\pi/4 - \delta)$ ו - $\theta_2 = \pm(3\pi/4 + \delta)$ כאשר $\delta = 1/2 \sin^{-1}(K_u / K_1)$. ניתן ליחס כיוונים אלה לאניזוטרופיה חד-צירית חלשה המתווספת בכיוון הציר הקשה של אניזוטרופיה דו-צירית. עבודה זו פורסמה ב:

Y. Bason, L. Klein, J.-B. Yau, X. Hong, and C. H. Ahn, physica status solidi Volume 1, Issue 12, Date: December 2004, Pages: 3336-3338.

תקציר

"אפקט הול המשטחי" התגלה כבר בשנות החמישים של המאה הקודמת, אך הוא פחות מוכר מ"אפקט הול הרגיל" ומ"אפקט הול המיוחד", בהם המתח הרוחבי המתפתח בדגם ניצב לזרם ולשדה המגנטי (אפקט הול הרגיל), או ניצב לזרם ולמגנטיזציה (אפקט הול המיוחד). באפקט הול המשטחי המתח הרוחבי נוצר במישור הדגם והשדה המגנטי, או במישור הדגם והמגנטיזציה. בנוסף, אפקט הול המשטחי הינו סימטרי תחת הפיכת השדה המגנטי או המגנטיזציה, בניגוד לאפקט הול הרגיל והמיוחד שהינם אנטי-סימטריים.

מקורו של אפקט הול המשטחי הוא בתלות ההתנגדות החשמלית בזוית שבין הזרם לשדה המגנטי, או בין הזרם למגנטיזציה, והוא מופיע במתכות ובחצאי מוליכים מגנטיים ולא מגנטיים. במוליכים מגנטיים, מקורו של אפקט הול המשטחי הוא בזוית בין המגנטיזציה לכיוון הזרם, תופעה הנקראת "anisotropic magnetoresistance" או AMR.

ה – AMR נובע מאינטראקצית ספין-מסלול של האלקטרון, המשפיעה בצורה שונה על כל חומר. בחומרים אותם חקרתי המודל המקובל לתיאור ה – AMR נקרא "מודל שני הערוצים של מוט". מודל זה מחלק את הזרם החשמלי במוליך לשני ערוצים, כאשר בכל ערוץ נושאי המטען הם אלקטרונים בעלי ספין שונה. ההתנגדות החשמלית שונה עבור הערוצים השונים, ותלוייה בזוית המגנטיזציה ביחס לכיוון תנועת האלקטרונים.

בחומרים פולי-קריסטליים (אמורפיים), בהם לא קיימים כיווני גידול מוגדרים לשריג ולכן רק כיווני המגנטיזציה והזרם החשמלי רלוונטים, ה- AMR מתבטא בתלות ההתנגדות החשמלית בצורה הבאה: $\rho = \rho_\perp + \left(\rho_\parallel - \rho_\perp\right)\cos^2\varphi$ כאשר $\rho_\parallel$ ו – $\rho_\perp$ הן ההתנגדויות עבור זרם מקביל או ניצב למגנטיזציה, בהתאמה, והזוית בין הזרם למגנטיזציה היא φ.

כאשר הזרם לא זורם במקביל או בניצב למגנטיזציה, ה – AMR יוצר גם מתח רוחבי, בדומה למתח הרוחבי הנוצר באפקט הול. אם נניח כי הזרם זורם בכיוון ציר x והמגנטיציה נמצאת במישור x-y ויוצרת זווית של φ בינה לבין הזרם, אז לשדה החשמלי בדגם יש גם רכיב אורכי: $E_{long} = \rho_\perp J + \left(\rho_\parallel - \rho_\perp\right)J\cos^2\varphi$ (הגורם להתנגדות האורכית – AMR) וגם רכיב רוחבי:

תוכן ענינים:

תקציר א
1 רקע תאורטי 1
1.1 אניזוטרופיה מגנטית 1
1.1.1 אניזוטרופיה תבניתית 1
1.1.2 אניזוטרופיה מגנטית 2
1.1.3 אנרגיה של אניזוטרופיה 2
1.1.4 חילוף מגנטי 4
1.2 התנגדות מגנטית אניזוטרופית ואפקט הול המשטחי 6
1.2.1 רקע תאורטי 6
1.2.2 ניתוח מתמטי 8
1.2.3 אפקט הול משטחי ענק 9
1.2.4 חילוף באפקט הול המשטחי 12
1.2.5 משואות מסדר גבוה 14
1.3 ספינטרוניקס 18
1.3.1 התנגדות מגנטית ענקית 19
1.3.2 התנגדות מגנטית ע"י מנהור 19
1.3.3 זכרון גישה אקראית מגנטי 20
1.3.4 זכרון גישה אקראית מגנטי מבוסס על אפקט הול המשטחי 23
2 חומרים 24
2.1 מנגניטים 24
2.1.1 התנגדות מגנטית כבירה 24
2.1.2 מבנה גבישי 26
2.1.3 דיאגרמות פאזה 26
2.1.4 מודל שכלוף כפול 27
2.2 מגנטיט 30
3 פרטי הניסויים 32
3.1 יצור שכבות דקות 32
3.1.1 מנגניטים 32
3.1.2 מגנטיט 33
3.2 הכנת הדגמים 33
3.3 ציוד 35
3.4 ניתוח נתונים 36
4 רשימת פרסומים 39
5 מאמרים 40
5.1 Giant planar Hall effect in colossal magnetoresistive $La_{0.84}Sr_{0.16}MnO_3$ thin films 40
5.2 Characterization of the magnetic anisotropy in thin films of $La_{1-x}Sr_xMnO_3$ using the planar Hall effect 44
5.3 Planar Hall-effect magnetic random access memory 48
5.4 Planar Hall effect in epitaxial thin films of magnetite 52
5.5 The magnetoresistance tensor of $La_{0.8}Sr_{0.2}MnO_3$ 55
בבליוגרפיה 61

עבודה זו נעשתה בהדרכתו של

פרופסור ליאור קליין

מן המחלקה לפיזיקה של אוניברסיטת בר-אילן

אפקט הול משטחי ענק במנגניטים

חיבור לשם קבלת התואר "דוקטור לפילוסופיה"

מאת:

יוסי בסון

המחלקה לפיזיקה

הוגש לסנט של אוניברסיטת בר-אילן

רמת גן שבט, תשס"ט